



## COUNTS OF GALAXIES IN A MERGER MODEL \*

P. Colin<sup>1</sup>, D.N. Schramm<sup>2,3</sup> and M. Peimbert<sup>1</sup>

<sup>1</sup>Instituto de Astronomía, Universidad Nacional Autónoma de México  
CP 04510 México, D.F. México

<sup>2</sup>The University of Chicago, 5640 S. Ellis Ave., Chicago IL 60637 USA

<sup>3</sup>NASA/Fermilab Astrophysics Center  
Box 500, Batavia, IL 60510 USA

### Abstract

A model for the photometric evolution of galaxies has been developed and has been applied to the problem of galaxy counts. The integrated colors of galaxies are calculated using the most recently computed evolutionary tracks from Maeder and collaborators complemented with evolutionary tracks derived by other authors. The asymptotic giant branch lifetime is left as a free parameter. A series of cosmological models using different values of the cosmological constant,  $\Lambda_0$ , and the density parameter,  $\Omega_0$ , have been computed. The universality hypothesis of the luminosity function of galaxies has been abandoned. The influence of galaxy merging on the counts has been considered in a simple manner by assuming that the number of strongly interacting galaxies in a comoving volume increases with redshift as a power law given by  $(1+z)^{3.8}$ . Taking a Schechter parametrization for the luminosity function of the different types of galaxies, we are able to reproduce the observations reasonably well. We have also considered models with a gaussian distribution for the luminosity function of the brighter galaxies that provide a poorer fit to the observations. It is shown that galaxy count data are not yet able to make unambiguous cosmological statements since evolutionary assumptions are critical. In particular, an  $\Omega_0 = 1$ ,  $\Lambda_0 = 0$  cosmology is shown to be consistent with the data.

---

\* submitted to *The Astrophysical Journal*



## 1. INTRODUCTION

The study of the time-dependent spectrophotometric properties of a galaxy has been done through the standard technique of evolutionary population synthesis (Tinsley 1980; Bruzual 1983; Arimoto & Yoshii 1986; Guiderdoni & Rocca-Volmerange 1987). The integrated stellar spectrum of a galaxy is computed once one knows the number and spectra of all stars located in the HR diagram. The quality of a population synthesis model relies primarily on the quality and completeness of the library of evolutionary tracks. Unfortunately, we do not have a complete, unique, and good library which produces evolutionary tracks for a wide range of metallicities; although the work of Maeder and collaborators (1992) does go in the direction of remedying this situation. In any case, we show that by building a good library and by making useful approximations one can produce a good population synthesis. With the new grids of evolutionary tracks by Schaller et al. (1993, hereafter SSMM) and the recent improvement in our understanding of the asymptotic giant branch (AGB) (Herman & Habing 1985; Lattanzio 1986; Bedijn 1988; Charlot & Bruzual 1991, hereafter ChB) we have the possibility to assemble a decent library of evolutionary tracks.

In this paper we use a standard procedure for the calculation of the color evolution of a galaxy; i.e., stars are binned in mass so that each mass bin is assigned to a fixed evolutionary track. The abrupt changes in the computed colors are eliminated by building a fine grid (in mass) of evolutionary tracks. In the limit of a continuous set of evolutionary tracks this standard method is equivalent to the isochrone synthesis one (ChB).

In addition to a good library of evolutionary tracks, two more ingredients are necessary: the star formation rate, SFR, and the initial mass function, IMF. They determine the type of object that the model computes. The standard procedure is to fit the observed colors of galaxies by using different star formation rates, galaxies of distinct Hubble type seem to have experienced different star formation histories (Kennicutt 1983). The fact that authors with different methods and different tracks, with their own particular metallicity considerations, each reproduce the observed colors of galaxies motivated the study of the photometric evolution of galaxies, paying attention to the star formation histories. For example, it is likely that numerous moderate redshift galaxy-like objects, which play a primary role in the number counts of galaxies (Cowie et al. 1993 and references therein), developed a very particular star formation rate. Moreover, it has recently been shown that it may be necessary to look for an episodic star formation rate, rather than a continuous one, which might account better for aspects like the age difference between the halo and the disk in our own galaxy (Wheeler, Sneden, & Truran 1989; Mathews & Schramm 1993; Colin & Schramm 1993) or the underabundance of oxygen observed in the Large Magellanic Cloud (Gilmore & Wyse 1991).

It has been suggested that the excess number of galaxies observed in the blue band (Tyson 1988; Metcalfe et al. 1991; Lilly, Cowie, & Gardner 1991), compared with the number predicted by a nonevolving model, might not be easily accounted for in a simple zero cosmological constant ( $\Lambda = 0$ ) model. The excess can be explained by introducing a cosmological constant (Fukugita et al. 1990), but it predicts simultaneously an excess number in the infrared band; this latter effect is diminished when one takes into account the finite size of the galaxy and the fact that we are not measuring the total magnitude (Yoshii 1993). Recent observations in the infrared, K, band leave us with a much reduced number of galaxies: in fact a nonevolving model with  $\Lambda = 0$  fits the data (Cowie et al. 1993; Cole, Treyer, & Silk 1992; Koo & Kron 1992; this paper) reasonably well. Another clue to solve the number count problem is found in the recent determinations of 187 redshifts in the  $20.0 \leq b_J \leq 21.5$  range of Broadhurst, Ellis, & Shanks (1988) and 87 redshifts in the  $21.0 \leq b_J \leq 22.5$  range of Colles et al. (1990). Although both samples are consistent with a nonevolving model, there are many uncertainties involved in the

observations (incompleteness, systematic errors, galaxy clustering, etc.) that one needs to be careful about before making any conclusions. Another effect that has to be taken into account is the blueing trend of the faint galaxies ( $B \gtrsim 22$ ): is this tendency provoked by the sudden emerging of a new population of galaxies? (Cowie et al. 1993; Cole, Treyer, & Silk 1992)

It seems that one may really be faced with an evolutionary problem rather than a cosmological one. In particular, we would like to show that a  $(\Omega_0, \Lambda_0) = (1, 0)$  model can reproduce all the observations. Such a model is supported by the fact that the excess in the number of galaxies in the blue is greater than that in the infrared. An attractive way to account for the relative excess of galaxies in the different bands, and one which has been recently explored, is the idea of galaxy merging (Guiderdoni & Rocca-Volmerange 1990; Carlberg & Charlot 1992). Guiderdoni & Rocca-Volmerange assume that the number density of galaxies per comoving volume increases with redshift due to mergers; their model suffers from the defect of not considering the counts in the K band. A recent work of Carlberg & Charlot (1992, hereafter CCh) about the evolution of the luminosity function of galaxies (LFG) explores the merging effects on the counts. Their model considers the brightening of the low-luminosity, rich-gas galaxies due to star formation bursts which occur as a result of mergers. CCh exploit the fact that in a cold dark matter scenario galaxies form prior to halo formation. The low-luminosity irregular galaxies have a greater ratio of gas mass to stellar mass and since mergers increase with redshift, one expects that this type of galaxy makes a significant contribution to the counts in the faint end.

The local luminosity function of galaxies contains about 1% of interacting galaxies (Toomre 1977). Carlberg (1990a,b) has shown that the fraction of merging galaxies increases with redshift. The merging rate is estimated from the fraction of the volume of the universe which has collapsed into objects of mass  $M$  or greater (Press & Schechter 1974). The merging idea is supported also by the observations of QSO absorption line systems which show evidence for galaxy-mass multiple cloud systems at high redshift (Turnshek 1989).

One of the ingredients present in any model for the number counts of galaxies is the luminosity function of galaxies. There is already sufficient observational evidence to show that this function is not universal; i.e., this function depends on the number density of galaxies of the region (field or cluster, or from cluster to cluster) (Sandage, Bingeli, & Tammann 1985, SBT; Bingeli, Sandage, & Tammann 1988, BST). In terms of the Schechter analytical representation of the LFG, this means that the parameters  $\alpha$  (the faint slope of the LFG) and  $M^*$  (the "knee" of the LFG) depend on the environment:  $\alpha \sim -1.0$  for field galaxies and  $\alpha \sim -1.25$  for the Virgo cluster (BST). This result is not unexpected: the LFG is considering all types of galaxies and it is known that each type of galaxy has a specific luminosity function (LF). Since each environment has a different mix of galaxies, their sum varies with galaxy density. Summarizing, a better choice for the LFG would be to consider for each type of galaxy, generally classified by its morphology (see Koo & Kron 1992 for another treatment of the problem), a different LF. In fact, it becomes of great importance when: a) one is studying the nature of the faint galaxies to explain the detected excess in the blue counts; and, b) one is fitting the low-redshift end of the redshift distribution, which strongly depends on the LF for the brighter galaxies.

## 2. PHOTOMETRIC EVOLUTION OF GALAXIES

### 2.1 Model

The goal here is to compute the color and magnitude evolution of galaxies, calling particular attention to the useful simplifications we have made in our construction of the library of evolutionary tracks. To compare our work with that of other authors,

we have calculated the evolutionary photometric properties of the galaxies with a rather standard star formation rate (SFR). On the other hand, more realistic star formation histories for the Galaxy, like the SFR of Mathews & Schramm (1993), are used in an attempt to model optimally the color evolution of late-type galaxies. The model, like others, utilized just one metallicity, the solar one. We believe this is reasonable for this initial exploration, since even though there are evolutionary tracks with different chemical compositions, these do not satisfy the homogeneity and completeness requirements. In the future, when a homogeneous and a complete set of evolutionary tracks, covering a wide range of metallicities, is available we will be able to elaborate our model of photochemical evolution of galaxies.

### 2.1.1 Stellar Birthrate Function

It is known that the stellar birthrate should be a function of time and stellar mass. However, in the absence of a complete understanding of the star formation process, and for reasons of simplicity, the stellar birthrate  $B(m, t)$  is often separated into two independent functions:

$$B(t, m) = \psi(t)\phi(m), \quad (2.1)$$

where  $\psi(t)$  denotes the star formation rate (SFR) and  $\phi(m)$  the initial mass function (IMF). Here we assume that the IMF is independent of time and space with a power law dependence on the mass; i.e.,

$$\phi(m) \propto m^{-(1+x)}, \quad (2.2)$$

under the following normalization,

$$\int_{m_{inf}}^{m_{sup}} \phi(m) dm = 1. \quad (2.3)$$

We use as inferior and superior limits of the IMF the following:  $m_{inf} = 0.1$  and  $m_{sup} = 60$ . For comparison purposes, a value of 1.35 for the exponent (Salpeter exponent) has been used, although we have considered other values.

As mentioned before, an exponential law for the SFR has been used in order to compare our results with those of other authors, in particular with the results of Bruzual & Charlot (1993, hereafter BCh); i.e.,

$$\psi(t) \propto \exp(-t/\tau), \quad (2.4)$$

where  $\tau$  is the star formation timescale. We have also investigated the evolutionary photometric properties under the unusual Mathews & Schramm SFRs, what we have called old and new Mathews & Schramm SFR (Colín & Schramm 1993). The old Mathews & Schramm SFR (OMS) is given by

$$\psi(t) = \begin{cases} A[re^{-t/t_0} - 1]e^{5t/3t_0} & t/t_0 \leq \ln r \\ B & t/t_0 \geq \ln r \end{cases}, \quad (2.5)$$

where  $\psi(t) \propto e^{2t/3t_0}$  for  $t/t_0 \ll \ln r$ ; and, the new Mathews & Schramm SFR (NMS) is given by

$$\psi(t) = a + b\delta(t - t_1)e^{-(t-t_1)/\tau_1} + c\delta(t - t_2)e^{-(t-t_2)/\tau_2}. \quad (2.6)$$

In both expressions, the parameters have to do with the characteristics that govern the behavior of the model which are: (i) a first burst followed by a more quiet star formation rate due to sporadic mergers and intrinsic quiescent star formation in the colliding clouds and (ii) a second burst as a result of the last major merger followed by the star formation

rate in the disk. We will not discuss further the origin and the phenomenology of these two SFRs but we refer the reader to Colín & Schramm (1993) and references therein.

### 2.1.2 Procedure

The usual procedure to compute the evolution of the integrated light of galaxies is pretty standard (Tinsley 1976; Bruzual 1983; Arimoto & Yoshii 1988), the gas mass that is transformed into stars during the time  $\Delta t = t_{i+1} - t_i$  is

$$\Delta M(t_i, t_{i+1}) = \int_{t_i}^{t_{i+1}} \psi(t) dt. \quad (2.7)$$

The SFR is normalized so that

$$\int_0^{T_g} \psi(t) dt = 1. \quad (2.8)$$

The number of main sequence stars of mass  $m_j$  formed out of  $\Delta M$  is given by

$$N(m_j) = \Delta M(t_i, t_{i+1}) \int_{m_1}^{m_2} \phi(m) dm, \quad (2.9)$$

where  $m_j$ ,  $j = 1, 2, \dots, n$ , is one of the masses for which an evolutionary track is available. The mass limits  $m_1$  and  $m_2$  are defined as

$$m_1 = \sqrt{m_j m_{j-1}}, \quad m_2 = \sqrt{m_j m_{j+1}}, \quad (2.10)$$

(Tinsley 1972; Bruzual 1983; Arimoto & Yoshii 1986). At the observed time,  $t$ , the stars which were born in this particular time interval,  $\Delta t$ , will have ages ranging from  $t - t_{i+1}$  to  $t - t_i$ . Let us assume that the stars of mass  $m_j$  live in their  $k$ th evolutionary stage from  $T_i$  to  $T_f$ . The number of stars of mass  $m_j$  that are in the  $k$ th evolutionary stage is given by the intersection of the time intervals  $(T_i, T_f)$  and  $(t - t_{i+1}, t - t_i)$ . Analytically, the number of stars in the  $k$ th stage at time  $t$  is given by

$$N_j^k(t) = \Delta M(T_1, T_2) \int_{m_1}^{m_2} \phi(m) dm, \quad (2.11)$$

where  $T_1 = \max(t - T_f, t_i)$  and  $T_2 = \min(t_{i+1}, t - T_i)$ . Obviously, when the intersection is null  $N_j^k(t) = 0$ , that happens if  $T_i \geq t - t_i$  or  $T_f \leq t - t_{i+1}$ . The total number of stars is found by adding those accumulated until time  $t$  in successive time steps. At every  $t$  the colors of the galaxy are computed by adding the luminosity of the stellar colors corresponding to the different positions in the HR diagram and weighted by the number of stars in each position.

## 2.2 Evolutionary Tracks

Recently, Schaller et al. (1993, hereafter SSMM) have computed a wide set of evolutionary tracks for stars in the mass range from 0.8 to 120  $M_\odot$  at  $Z = 0.020$  and  $Z = 0.001$ . The models use the new opacities of Rogers & Iglesias (1992) for  $T \geq 6000$  °K and for lower temperatures use those of Kurucz (1991). Important physical parameters such as the nuclear reaction rates and the neutrino loss rates have been updated. The mixing length and the overshooting parameter change as a consequence of the new opacities. A detailed treatment of the partial ionization has been considered; in particular, their models take

into account, the ionization due to pressure. This effect modifies the values of the stellar parameters in the red giant branch (see below).

Similar to the Maeder & Meynet (1989, hereafter MM) tracks, the Schaller et al. tracks are incomplete in the sense that they do not consider several stages of late stellar evolution. To build our library of tracks we have proceeded in the following manner:

1. As in MM, SSMM stop their models for low-mass stars, from 0.8 to 1.7  $M_{\odot}$ , at the tip of the red giant branch. These tracks are completed approximating the He burning stage by an empirical formula of Lattanzio (1986) for the calculation of the luminosity and effective temperature, with lifetimes taken from Seidel, Demarque, & Weinberg (1987). We consider this a good fit because the HR parameters remain almost constant during the helium burning (down to central helium abundance  $Y \sim 0.05$ ). Based on the assumption that the T versus L behavior of the early AGB stage, E-AGB, is quite linear, we have connected the helium exhaustion point to the beginning of the thermal pulse AGB stage, TP-AGB, by a straight line. The lifetime of the E-AGB is taken as a free parameter of the model.

2. SSMM do not go beyond the E-AGB for intermediate mass stars, from 2.0 to 5.0  $M_{\odot}$ . We have added a point to take into account the TP-AGB, the so called OH/IR stage for intermediate and low mass stars (ChB). The luminosity and lifetime of this phase are from Bedijn (1988) and the effective temperature is from Lattanzio (1986) and Becker & Iben (1979).

3. SSMM do not complete the red giant branch for stars of 0.9 and 0.8  $M_{\odot}$ . The 0.8  $M_{\odot}$  model is not important for our purposes, because the main sequence lifetime is greater than the age of the universe. Alternatively, the 0.9  $M_{\odot}$  model is very important because the present colors of an elliptical galaxy depend on the luminosity of the 0.9  $M_{\odot}$  model in the red giant branch. We have used the 0.9  $M_{\odot}$  model calculated by Schaller (private communication).

4. The main sequence stage, MS, is extrapolated down to 0.7  $M_{\odot}$  and for masses in the  $0.1 M_{\odot} < m < 0.7 M_{\odot}$  the unevolving models of Tinsley & Gunn (1976) are used. We have also calculated models using the very low-mass evolutionary tracks ( $0.1 M_{\odot} \leq m \leq 0.75 M_{\odot}$ ) of Vandenberg et al. (1983) and obtained similar results.

In total, we end up with 19 evolutionary tracks which go from the zero age main sequence to TP-AGB or to central carbon exhaustion, for masses greater than 5  $M_{\odot}$ . To avoid abrupt changes in the computed evolutionary photometric properties we have incorporated 791 interpolated tracks to our library. Our interpolation scheme takes points with the same physical significance from any two neighboring (in mass) tracks and interpolate linearly in the logarithm of the physical parameters to produce more tracks. Care must be taken when interpolations involving masses close to the following ones masses are carried out:  $M_C$ ,  $M_{HeF}$  and  $M_{up}$ . The first mass denotes the lower limit where a convective core is still found,  $1.0 M_{\odot} < M_C < 1.25 M_{\odot}$ . The second one represents the limit above which a star ignites helium quietly,  $1.7 M_{\odot} < M_{HeF} < 2.0 M_{\odot}$ . And finally,  $M_{up}$  is the maximum mass limit for degenerate C-ignition,  $M_{up} \approx 7.0 M_{\odot}$ . The given numbers are for the stellar models of SSMM for  $Z = 0.020$ . For simplicity, a single metallicity calculation is done in the models.

### 2.2.1 Color-Magnitude Diagram

The transformation of the theoretical HR diagram to the observational color-magnitude one is done by using the standard calibrations of Johnson (1966), Lee (1970), and Flower (1977). The colors in the UBVRIJKL photometric system are calculated from Johnson (1966) and Lee (1970). All main sequence stars are class V, stars whose luminosity logarithm,  $\log L$ , in solar luminosity units is less than 3.5 are class III (giants), and those

with  $\log L$  greater than 3.5 are Ia or Ib (supergiants) (Becker & Mathews 1983). For temperatures greater than the maximum value of Flower's calibration we compute the colors from black body calculations. Particular emphasis should be put on the computation of the TP-AGB colors. Stars in this stage drive strong winds which produce a circumstellar shell. The light coming from the OH/IR stars is very reddened due to the circumstellar dust. To take this effect into account, we followed the idea of ChB to compute the colors; in particular, we assume that all stars on the upper side of TP-AGB (OH/IR phase) have the colors of one prototype star, IK Tau; this star has color indexes representative of the observed OH/IR (Reid, Tinney, & Mould 1990). Its bolometric correction was calculated using the observed fluxes, in the optical and in the near infrared from Dyck et al. (1974) and in the far infrared from Herman, Burger, & Phennix (1986).

### 2.3 Results

The observed values of the color indexes, from U-V to V-L, of the elliptical galaxies (taken from a compilation of Yoshii & Takahara 1988) are shown in Table 1. For comparison, we also show in Table 1 the synthesized colors for a burst star formation rate, simulated here as a SFR that is constant during the first  $10^9$  yr and zero after. By considering a burst functional form for the SFR what we try to do is to fit the colors of an elliptical galaxy (Bruzual 1983, ChB), where one knows that if there is current star formation it is very small. With Ch we have denoted the synthesized colors using the low-mass evolutionary tracks (from 0.6 to  $1.0 M_{\odot}$ ) of Chiosi (1992). It is worth mentioning here that the stellar population of the bulge of the Galaxy, we believe, reflects better the stellar population of elliptical galaxies. This is due in part to the average supersolar metallicity we find in this type of galaxy. Having this in mind, we have computed the colors of the late red giants evaluating their absolute magnitude, in the visual, using the data from Frogel & Whitford (1987) and shifting the photometric calibration of Lee (1970) by three spectral subclassifications; for example, the color index V-K associated with M4 will have the temperature associated with M1 in the Lee (1970) calibration. To get V-K as red as 3.3 we have reddened the colors by increasing the lifetime of the late red giants of the 0.9 and  $1.0 M_{\odot}$  models. The total lifetime of the models is not modified because when we increase the duration of the giant phase, we decrease the lifetime of the main sequence phase accordingly.

The evolution of the color indexes B-V and V-K for a burst, constant, and exponentially decreasing ( $\tau = 0.5$  Gyr) SFR are plotted in the Figs. 1a-1b. The Salpeter exponent for the IMF has been used. From the figures, we can see clearly the tendency to redder colors once we stop the star formation process (line with a burst SFR); the reddening with the exponentially decreasing SFR is more gradual, although it reaches values as high as the burst SFR. Our results differ from those of BCh in various aspects: first, BCh get a value for V-K of  $\sim 0.2$  greater during the first 1 Gyr (period in which the SFR is constant); second, BCh have two local minima, again in V-K, at  $\sim 2.0$  Gyr and at  $\sim 7.0$  Gyr; and, third, the reddening in B-V is more pronounced in our models. The major differences are due to the evolutionary tracks and the photometric calibration we are using. In Figs. 2a-2b the same models are plotted but in this case we have added our models with the calibration for lower temperatures provided kindly to us by Bruzual. As one can see from the figures, the differences between Bruzual's models and ours are smaller; the differences can be attributed to: a) the models of BCh use a different mass range for the IMF (from 0.1 to  $125 M_{\odot}$ ); b) differences in the way to complete the low-mass and intermediate-mass evolutionary tracks; c) the form used to compute the stellar parameters for very low-mass stars and its consequent transformation to the observational HR diagram; and d) although we do not believe it is significant, the differences between the MM tracks (using the corrected timescale) and those of SSMM. That our V-K takes values as red as  $\sim 3.2$  mag at  $\sim 10$  Gyr is independent of the chosen calibration and it is due to these factors:

first, the stellar population of the bulge of our galaxy has been taken as representative of the stellar population of an elliptical galaxy, and, second, we have increased the lifetime of the red giant branch.

To demonstrate the “kindness” of our standard method in the calculation of the color indexes or magnitudes, when a fine division of the interpolated tracks is considered we have plotted in Figs. 3a-3b the evolution of B-V and V-K for a  $10^8$  yr burst SFR (Bruzzi’s calibration). The discontinuous changes, which one would otherwise observe, are eliminated by considering a fine division in the computed tracks (see ChB).

In Figs. 4a-4b the evolution of the color indexes B-V and V-K for the two Mathews and Schramm SFRs are plotted. As it is clear from the figures, one can reproduce the present colors of the galaxies with very different star formation histories, this might have an appreciable effect on the number counts of galaxies. Notice how the curves with a constant SFR begin to redden once the contribution of the red giants starts to be significant ( $\sim 1$  Gyr). Comparing our synthesized colors with the observed ones, for spiral and irregular galaxies, the former appear less reddened. This is probably due to the dust contribution that we are not taking into account in the models.

In the color-color diagram of Figs. 5a-5b, V-K versus B-V has been plotted for different star formation rates. The point in Fig. 5a is the calculated value with Chiosi’s low-mass tracks at  $t = 15$  Gyr. What can we conclude from the diagram? It is indicating to us that the greater reddening observed in elliptical galaxies is not reproduced simply by increasing the lifetime of the red giant branch; in fact, even using Chiosi’s low-mass tracks, we are still having problems in fitting the average colors. Perhaps, we will have an answer when the post-asymptotic giant branch or some missing supersolar metallicity evolutionary phase is taken into account (Renzini 1993).

### 3. NUMBER COUNTS OF GALAXIES

#### 3.1 Model

A model of counts of galaxies should include: a) an appropriate cosmological model for the distance and volume elements, both quantities depending on the redshift,  $z$ , the density parameter,  $\Omega_0 = \rho/\rho_c$  ( $\rho_c \equiv 3H_0^2/8\pi G = 1.879h^2 \times 10^{-29} \text{ g cm}^{-3}$ ), and the cosmological constant,  $\Lambda_0$ ; b) a magnitude-redshift relationship, including the  $k$  and  $e$ , evolutionary correction; and, c) a luminosity function of galaxies including all types of galaxies as well as a possible evolution of the number density per comoving volume. Therefore, in order to search for some cosmological effect through the counts of galaxies, it is extremely important to examine first the effects on the counts by the evolution of the luminosity function of galaxies.

#### 3.1.1 Procedure

The number of galaxies per unit area is obtained by counting all galaxies over various finite areas of the sky. If  $n(m_\lambda, z)dm_\lambda dz$  represents the number of galaxies in  $m_\lambda$  and  $m_\lambda + dm_\lambda$  and in  $z$  by  $z + dz$  then

$$n(m_\lambda, z) = \omega \frac{dV}{dz} \sum_{i=1}^n \Phi^i(M_\lambda, z), \quad (3.1)$$

where  $\omega$  is the solid angle over which the galaxies are counted,  $\frac{dV}{dz}$  is the cosmological volume element,  $n$  is the number of type of galaxies, and  $\Phi^i(M_\lambda, z)$  is the luminosity function of galaxies (LFG). Here, it is convenient to mention that the scheme we are

dealing with is the 100% detection and total magnitude one (Yoshii 1993). The absolute magnitude in the “ $\lambda$ ” band,  $M_\lambda$ , is related to the apparent magnitude  $m_\lambda$  by:

$$M_\lambda = m_\lambda - k_\lambda(z) - e_\lambda(z) - 5\log(d_L(z)/10^{-5} \text{ Mpc}), \quad (3.2)$$

where

$$k_\lambda(z) = 2.5\log(1+z) - 2.5\log\left(\frac{\int_0^\infty f_{\frac{\lambda'}{1+z}}(0)R_\lambda(\lambda')d\lambda'}{\int_0^\infty f_{\lambda'}(0)R_\lambda(\lambda')d\lambda'}\right), \quad (3.3)$$

and

$$e_\lambda(z) = -2.5\log\left(\frac{\int_0^\infty f_{\frac{\lambda'}{1+z}}(z)R_\lambda(\lambda')d\lambda'}{\int_0^\infty f_{\frac{\lambda'}{1+z}}(0)R_\lambda(\lambda')d\lambda'}\right). \quad (3.4)$$

With  $k_\lambda$  and  $e_\lambda$  we have denoted the correction factors, to the apparent magnitude, due to the redshift and length contraction,  $k$  correction, and due to the luminosity evolution of the galaxies,  $e$  correction. In eqs. (3.3) and (3.4) we have denoted with  $f_\lambda$  the spectral energy distribution for each type of galaxy and with  $R_\lambda$  the response function of the filter. Integrating (3.1) from  $z = 0$  to  $z = z_F$ , we get the number of galaxies per unit magnitude,

$$n(m_\lambda) = \int_0^{z_F} n(m_\lambda, z) dz, \quad (3.5)$$

where  $z_F$  is the galaxy formation redshift.

### 3.1.2 Cosmology

The distribution of matter and radiation in the observable universe is highly homogeneous and isotropic. While this does not guarantee that the *entire* universe is homogeneous, it implies that the region covered by the observable universe is smooth (the observable universe  $\sim$  Hubble distance  $= cH_0^{-1} = 9.25 \times 10^{27} h^{-1} \text{ cm}$ ). Since the universe is homogeneous and isotropic on the scale of the Hubble volume, for description purposes we assume that the entire universe is homogeneous and isotropic. Anisotropy in the background radiation field of  $1.1 \pm 0.2 \times 10^{-5}$  at  $10^\circ$  has been recently detected by the COBE satellite. The line element that describes a homogeneous and isotropic space is the Robertson-Walker metric and it is given by

$$ds^2 = dt^2 - R^2(t) \left\{ \frac{dr^2}{1 - kr^2} + r^2 d\theta^2 + r^2 \sin^2 \theta d\phi^2 \right\}, \quad (3.6)$$

where  $(t, r, \theta, \phi)$  are comoving coordinates,  $R(t)$  is the cosmic scale factor, and  $k$  is equal to  $+1$ ,  $-1$ , or  $0$  (the curvature term). The volume element is given by,

$$dV = \sqrt{h} d^3x = \frac{R^3(t_0)r^2}{\sqrt{1 - kr^2}} dr d\omega, \quad (3.7)$$

where  $h$  is the determinant of the line element and  $R(t_0) = R_0$  the scale factor at the present time. Rewriting eq. (3.7),

$$\frac{dV}{d\omega dz} = \frac{R^3(t_0)r^2(z)}{\sqrt{1 - kr^2(z)}} \left( \frac{dr}{dz} \right). \quad (3.8)$$

The distance to a luminous source  $d_L$  is defined through the relation  $\mathcal{F} = \frac{\mathcal{L}}{4\pi d_L^2}$ , where  $\mathcal{L}$  is the absolute luminosity of the source in its rest frame system and  $\mathcal{F}$  is the energy flux measured by the detector. The observed flux is given by

$$\mathcal{F} = \frac{\mathcal{L}}{4\pi R^2(t_0)r^2(1+z)^2}, \quad (3.9)$$

and

$$d_L^2 = R^2(t_0)r^2(1+z)^2. \quad (3.10)$$

The functional form of the coordinate  $r$  with  $z$  is determined through the equality

$$\int_t^{t_0} \frac{dt}{R(t)} = \int_0^r \frac{dr}{\sqrt{1-kr^2}}, \quad (3.11)$$

which can be written, after using one of the Friedmann equations (see, e.g., Kolb & Turner 1990 for a review of standard cosmology) and the relation  $R = R_0(1+z)^{-1}$ , of the following manner:

$$\frac{c}{R_0 H_0} \int_{(1+z)^{-1}}^1 \frac{dx}{x \sqrt{\Omega_m x^{-1} + \Omega_v x^2 - \frac{c^2 k}{H_0^2 R_0^2}}} = \int_0^r \frac{dr}{\sqrt{1-kr^2}} \quad (3.12)$$

where  $\Omega_v = \rho_v/\rho_c$  is the contribution of the vacuum to the energy density and is related to the cosmological constant by  $\Lambda = 8\pi G\rho_v$ . The eqs. (3.8) and (3.12) are constrained by

$$1 = \Omega_m + \Omega_v - \frac{c^2 k}{H_0^2 R_0^2}. \quad (3.13)$$

Taking the derivative of eq. (3.12) with respect to  $z$  and inserting the result in the volume element formula we get

$$\frac{dV}{d\omega dz} = \left(\frac{c}{H_0}\right) R_0^2 \frac{r^2}{1+z} \frac{1}{\sqrt{\Omega_m(1+z) + \Omega_v(1+z)^{-2} - \frac{c^2 k}{R_0^2 H_0^2}}}. \quad (3.14)$$

The explicit form for  $r(z)$  depends on the  $k$  value; for example, if  $k = -1$  the right hand side of the eq. (3.12) is equal to  $\sinh^{-1} r$  and  $r(z)$  is simply

$$r = \sinh \left( \frac{c}{R_0 H_0} \int_{(1+z)^{-1}}^1 \frac{dx}{x \sqrt{\Omega_m x^{-1} + \Omega_v x^2 + \frac{c^2}{H_0^2 R_0^2}}} \right), \quad (3.15)$$

where  $\frac{c^2}{H_0^2 R_0^2} = 1 - \Omega_m - \Omega_v$ . On the other hand, the age of a galaxy,  $t_G$ , and the cosmic time are related to each other by

$$t_G(z) = t(z) - t(z_F), \quad (3.16)$$

where

$$t(z) = \frac{1}{H_0} \int_0^{(1+z)^{-1}} \frac{dx}{\sqrt{\Omega_m x^{-1} + \Omega_v x^2 - \frac{kc^2}{H_0^2 R_0^2}}}. \quad (3.17)$$

### 3.1.3 “k + e” Correction

To evaluate the “k + e” correction, eqs. (3.3) and (3.4), the spectral energy distribution (SED) for each type of galaxy and the response function for each color band are needed. If the energy flux were a power law, that is  $f_\lambda \propto \lambda^\nu$ , the k correction would be given by the simple formula  $k_\lambda(z) = 2.5(1 + \nu)\log(1 + z)$ ; in particular, if  $\nu = -1$  then  $k_\lambda(z) = 0$ . The SEDs considered are from Coleman, Wu, and Weedman (1976, hereafter CWW) and Pence (1976) for Sab galaxies. The SED for elliptical galaxies is taken from the SED of the bulge of M31. The fluxes beyond  $1 \mu m$  are computed, like Yoshii & Takahara (1988, hereafter YT), using our synthesized colors: the evolution of the flux,  $f_\lambda(z)$ , is following through the evolution of the colors. Two points related to  $k_\lambda(z)$  and  $e_\lambda(z)$  calculations should be mentioned before going on: first, we do not know the values of the SEDs for  $\lambda \leq \lambda_{inf}$  ( $\lambda_{inf} = 0.13 \mu m$ ) and therefore we have assumed  $f_\lambda = f_{\lambda_{inf}}$  from  $\lambda = 0.0912 \mu m$  to  $\lambda_{inf}$ ; second, we can only evaluate  $f_\lambda(z)$  for  $\lambda \geq \lambda_U$  ( $\lambda_U = 0.36 \mu m$ ) from our photometric code and, therefore, as a first approximation, it is assumed that  $f_\lambda(z) = f_\lambda(0) \left( \frac{f_{\lambda_U}(z)}{f_{\lambda_U}(0)} \right)$  for  $\lambda \leq \lambda_U$ . The first point affects the k correction, although its effect is negligible when a small value for  $z_F$  is assumed, like the one used here; actually, higher values for  $z_F$  may have assumed without affecting the K band k correction at all. The second point affects the e correction in the B band.

### 3.1.4 Luminosity Evolution of Galaxies

As was mentioned in the last section, to compute the evolutionary correction, it is necessary to obtain the spectral energy distribution as a function of  $z$ . It was also noted that our photometric evolution of galaxies (PEG) model provides us the approximate SEDs for wavelengths longer than  $\lambda_U$ ; for  $\lambda \leq \lambda_U$  we assumed that the shape of the SEDs did not change and that their amplitude scaled with the value of the flux at  $\lambda_U$ . It is evident that if the ratio  $f_\lambda/f_{\lambda_U}$  for  $\lambda \leq \lambda_U$  increases with  $z$ , one is sub-estimating the e correction, with consequent effects on the faint end of the blue band counts.

Let us see now how to compute  $f_\lambda(z)$  from the SEDs and our photometric code. First of all, starting from the relation  $m_\lambda = -2.5\log f_\lambda + cte.$  we find

$$\log f_{\lambda'}(0) = \log f_\lambda(0) + \log \left( \frac{f_{\lambda'}^0}{f_\lambda^0} \right) - 0.4(m_{\lambda'} - m_\lambda), \quad (3.18)$$

where  $f_\lambda^0$  satisfies  $m_\lambda(f_\lambda^0) \equiv 0$  (see, e.g., Johnson 1966); as in YT, it is assumed that  $\lambda = \lambda_R = 0.7 \mu m$ . From eq. (3.18) we obtain  $f_{\lambda'}^0$  for near infrared wavelengths, using the synthesized color indexes V-J, V-K, and V-L and the value of  $f_{\lambda_R}$  from the “observed” SEDs. The resulting SEDs from  $\lambda = 0.0912$  to  $3.4 \mu m$  are plotted in Fig. 6. Second, once one has calculated  $f_\lambda(0)$ , the flux energy for any value of  $z$  is obtained through the relation

$$\log f_\lambda(z) = \log f_\lambda(0) - 0.4(M_\lambda(z) - M_\lambda(0)), \quad (3.19)$$

where  $M_\lambda(z)$  denotes the absolute magnitude in the “ $\lambda$ ” band computed from our PEG.

The evolution of the luminosity, in the different color bands, has been calculated, describing the different type of galaxies through standard assumptions for the functional form of the IMF and the SFR. A power law with the Salpeter exponent has been used for the IMF and an exponentially decreasing law SFR, varying the time scales to take into account the distinct types of galaxies (ChB). In a future paper we are going to explore the effects on the counts when various nonstandard SFRs are assumed. Table 2 shows the synthesized color indexes, from U-V to V-L, (( $\Omega_m, \Omega_v$ )=(1,0) model) along with the

observed ones (taken from a compilation of YT) for the different types of galaxies. The distinct types of galaxies E/S0,...,Sdm are modeled with the following time scales for the SFR: 0.5, 3.0, 5.0, 9.0,  $\infty$  ( $\times 10^9 yr$ ), respectively.

As we mentioned before, the differences between the synthesized colors and the observed ones are very probably due to the absence of the following: first, dust in our models (Wang 1991); second, the post-asymptotic giant branch (BCh) and another possible evolutionary phase (Renzini 1993); and, third, an updated photometric calibration.

The k, e, corrections and their sum, in the B and K, bands are plotted in Figs. 7a-7f for the distinct types of galaxies, for the  $(\Omega_m, \Omega_v) = (1, 0)$  model and  $z_F = 3$ . As observed from Fig. 7a, the k correction increases when models move from late galaxies to early ones. This is due to the variation in the flux contribution to the ultraviolet region. In particular, we see how, for the late galaxies, the k correction is almost zero. As far as the e correction is concerned (Fig. 7b), the biggest effect is seen again in the earlier galaxies. This is what one would expect because the luminosity evolution follows the history of the star formation rate. The greater the time scale of the SFR, the lower is the effect on the e correction. The sum of both effects (Fig. 7c) is kept to  $\pm 1$  magnitude range, except for the E/S0 galaxies.

### 3.1.5 Luminosity Function of Galaxies

As was pointed out in the introduction, there is already enough observational evidence that proves that the luminosity function of galaxies (BST) is not universal. The LFG depends on the number density of galaxies of the considered region. However, the assumption of universality for each type of galaxy seems to be a good hypothesis; within the uncertainties, we can say that the shape of the luminosity function (LF) for each type of galaxy does not change when we pass from a high-density region (Virgo cluster) to a low-density one (local field).

Like other authors (YT, CCh) we have divided galaxies in five morphological classes: E/S0, Sab, Sbc, Scd, and Sdm, each one described by the Schechter (1976) functional form for the LF:

$$\Phi(M)dM = 0.92\Phi^* \exp\{-0.92(\alpha + 1)(M - M^*) - \exp[-0.92(M - M^*)]\}dM. \quad (3.20)$$

Unlike YT, CCh do take into account the non-universality of the LFG. They assume different values for the ‘‘Schechter’’ parameters  $\alpha$  and  $M^*$ . We have computed counts of galaxies models utilizing different assumptions about  $\Omega_m$ ,  $\Omega_v$ , LFG and the mix of galaxies. In particular, the hypothesis of universality of the LFG has been used, although it has become more difficult to sustain. In addition, models that drop this assumption have also been computed.

Making use of the ‘‘k + e’’ correction and the universality hypothesis, we have followed the ‘‘passive’’ evolution of the LFG in Fig. 8 for a flat and a zero cosmological constant universe. Simply,

$$\Phi(M_\lambda, z) = \Phi M_\lambda - [k_\lambda(z) + e_\lambda(z)], 0, \quad (4.21)$$

where  $M_\lambda = m_\lambda - 5 \log(d_L(z)/10^{-5} Mpc)$ . The behavior of the evolution of the LFG can be understood if one goes back to Figs. 7a-7f. The LFG moves first to the left because the ‘‘k + e’’ correction is positive for all types of galaxies. The evolution of the LFG changes its tendency from moving left to going right due to the following factors: first, the Sab ‘‘k + e’’ correction becomes negative; and, second, the E/S0 ‘‘k + e’’ correction starts diminishing, becoming negative for high  $z$  values.

In addition to the ‘‘passive’’ evolution of the LFG, one might expect an ‘‘active’’ evolution in which the shape and/or the normalization (which gives the total number per

comoving volume) of the LFG would vary. There are at least three possible active evolutions: a) the slope of the LFG,  $\alpha$ , increases with  $z$ , maintaining a constant number, i.e., the low-luminosity population increases at the cost of decreasing high-luminosity population; b) the lower luminosity limit increases to brighter magnitudes with  $z$ , meaning that galaxies in the past were brighter, possibly due to strong bursts of star formation; c) drop the hypothesis of conserving numbers of galaxies and assume that it increases with  $z$ , perhaps due to mergers. These effects are very probably related to each other; for example, the merging hypothesis would imply the nonconservation of the number of galaxies and appreciable changes in the intrinsic luminosity of galaxies (CCh).

### 3.2 Counts of Galaxies in a Traditional Model

In Table 3 we have gathered the different parameters which play a role in the calculation of the number of galaxies versus redshift or magnitude. The first three columns correspond properly to the cosmological parameters; the fourth column corresponds to the redshift of galaxy formation; the fifth and sixth columns are the functions that determine the stellar evolution of a galaxy; the seventh column gives the number of galaxy types; the eight, ninth, and tenth columns are the parameters associated with the LFG; the eleventh column gives the mix used; and the twelfth column gives the universality hypothesis. Among the different parameters in Table 3 we have fixed:  $h$ ,  $z_F$ ,  $n_{tg}$ , and the functional form of the SFR and the IMF. Like CCh we have abandoned the hypothesis of universality in some of our models.

The number density of galaxies against blue apparent magnitude ( $B_J$ ) has been plotted in Fig. 9 assuming universality for the LFG. The data are from Maddox et al. (1990), Metcalfe et al. (1990), and Lilly et al. (1991). The different lines cover evolving and nonevolving models. Several comments about the figure are pertinent: first, as mentioned earlier in numerous papers, the nonevolving models start running away from the observations at about  $B \sim 21$ ; second, the  $(\Omega_m, \Omega_v) = (1, 0)$  model does not reproduce the data; and, third, the blue counts favor open or nonzero cosmological constant cosmologies. In Fig. 10, besides repeating the  $(\Omega_m, \Omega_v) = (1, 0)$  model (solid line), the contributions from the different galaxy types are considered separately. The difference between one curve and another should be sought in the different contributions to the local LFG and the developing of the "k + e" correction for each type of galaxy; for example, although E/SO galaxies contribute most to the LFG, they are less favored than Sab or Sbc galaxies, in a number versus magnitude plot, due to their bigger "k + e" correction. Figure 11 is similar to Fig. 10 except that here we have changed the mix and the normalization parameter. In addition, we have used the parameters of CCh for the LFG. In this case, the E/SO are the brightest galaxies and, therefore, they contribute most (almost 100 %) at the bright end. Comparing the results in Fig. 11 with those in Fig. 10, it is seen in Fig. 11 that the greater contribution, at faint magnitudes ( $B_J \sim 27$ ), is due to Scd and Sab galaxies. The contribution from Sdm galaxies is beginning to be significant

The number-magnitude relation in the K band has been plotted in Fig. 12, keeping the same line code of Fig. 9. The data are from Cowie et al. (1993). Unlike the results in the blue band, here the models which best fit the observations are the nonevolving ones; the evolving models with open or nonzero cosmological constant cosmologies predict an excess of galaxies. Even more, in a number-redshift plot, for a given magnitude interval, the evolving models produce an excess of high  $z$  galaxies (see Fig. 13). The different curves in Fig. 13 are the models for which a number versus magnitude plot has been drawn before. The observations are taken from Broadhurst, Ellis, & Shanks (1988). These results, along with those of Fig. 12, support the idea that the problem of the excess of galaxies, seen in the blue counts, is evolutionary rather than cosmological; in particular, we should not reject the  $(\Omega_0, \Lambda_0) = (1, 0)$  model, before revising all the hypotheses involved in this kind of

calculation.

### 3.2.1 Counts of Galaxies in a Merger Model

This section describes a simple  $(\Omega_0, \Lambda_0)=(1,0)$  model which, among other things: abandons the universality hypothesis of the LFG; divides the galaxies in the following five classes: E/SO, dE/dSO (spheroidal dwarfs), Sa-c (spirals), dI (dwarf irregulars), and I (interacting galaxies); uses two different representations for the LF of brighter galaxies (E/SO and Sa-c), a gaussian and a Schechter distribution; and, finally, proposes that the number density per comoving volume increases as a power law  $\phi^* \propto (1+z)^\eta$ . The I class has been represented in the following manner: its spectral energy distribution is that of an irregular galaxy, Sdm class according to CWW. In a future paper, we will be using the SED of a galaxy like NGC 605 (strongly interacting galaxy) which, we think, would better represent this class. We have also assumed that the luminosity of the I class does not change with time; i.e., regardless of their origin and epoch in which they are seen, the luminosity function of the I galaxies does not change with time, except for the k correction. The dI class has been also represented by a SED of an irregular galaxy and with a time scale for the SFR of 15 Gyr. We have assumed a Schechter function for its LF with  $\alpha = -1.4$  and  $M^* = -16.2$ . The Sa-c class has the Scd (CWW) SED and a time scale of 6 Gyr for the SFR. Its LF has been represented by a gaussian distribution with the parameters,  $\sigma = 1.5$  and  $M^* = -18.4$  (SBT), although for comparison we have also used the Schechter parameters  $\alpha = -1.00$  and  $M^* = -19.0$ . The SED of the dE/dSO class is assumed to be the one for the Sab group with a SFR time scale of 5.0 Gyr. Since we know that this type of galaxy is of low-metallicity ( $-2 \lesssim [\text{Fe}/\text{H}] \lesssim -1$ , Caldwell et al. 1992) and with an average B-V color of  $0.75 \pm 0.04$ , one is automatically unable to model these galaxies with a solar-metallicity photometric code; nevertheless, we believe we have given a fair representation for them. Its Schechter parameters are  $\alpha = -1.35$  and  $M^* = -18.0$  (SBT). Finally, we have come to the E/SO class. According to Ferguson & Sandage, (1991) a better analytical representation for its LF is a gaussian distribution, at least for the LFs of the nearby cluster of galaxies. Therefore we have considered the values for  $\sigma$  and  $M^*$  to be 1.5 and 18.8, respectively, which coincide with the Virgo cluster (Ferguson & Sandage 1991). Like the group of spiral galaxies, we have also used a Schechter formulation for its LF. The values of the parameters  $\alpha$  and  $M^*$  are -0.5 and -20.5, respectively. As we will see, the Schechter representation for the LFs of the brighter galaxies, E/SO and Sa-c, gives a much better fit to the number-redshift relation, maintaining the good fit on the number-magnitude relation. This is something that had not been noted before and therefore should be emphasized.

In Figs. 14a-14b we have plotted the number of galaxies against blue apparent magnitude, with the previously cited parameters, for the two representations of the LF for brighter galaxies. The exponent  $\eta$  which we found fits the observations better is 3.8. The different lines are the contribution to the total number, the solid line, from the distinct types of galaxies. Even though the two models reproduce the observations reasonably well, they differ from each other in the contribution of the brighter galaxies to the total number. In Fig. 14a, with the gaussian representation of the LF for the brighter galaxies, the three brighter classes contribute with almost the same weight, while in Fig. 14b, with the Schechter formulation, the E/SO class is what contributes most (bright end). The number of galaxies versus K apparent magnitude is plotted in Figs. 15a-15b. In both figures it is notable that the counts are almost exclusively coming from E/SO galaxies, at least up to  $K \sim 19$ . One differs slightly from the other at  $K \sim 18$ . The redshift distribution of galaxies, in the B band, for the two intervals  $20.0 < b_J < 21.5$  and  $20.0 < b_J < 21.0$  is plotted in Figs. 16a-16b for the two representations. The solid line denotes the gaussian representation and the data are from Broadhurst et al. (1988). As we mentioned before, we see clearly how a Schechter formulation for the LF of the brighter galaxies (E/SO and

Sa-c classes) reproduces the observations better. This is simply due to the fact that, in the gaussian representation, the brighter part of the logarithm of the LF drops as the square whereas in the Schechter formulation it drops exponentially. Although the model with a gaussian representation does not reproduce the observations, it produces an excess of high  $z$  galaxies. Nevertheless, one should not forget that the greater uncertainties are located at the high  $z$  and at the faint end. Therefore, it is possible that the model "excess" is really a "deficit" in the observed number.

#### 4. CONCLUSIONS

We have shown that a standard evolutionary synthesis population model does not produce abrupt changes in the calculation of the luminosity evolution when a very fine mass-track red is used. In this sense the standard method is equivalent to the isochrone synthesis one. Our results are consistent with those of ChB and BCh, although differences are observed. These differences are due to two different aspects: first, approach of the problem and different input parameters, and second, absence of the PAGB and updated photometric calibration for low temperatures. Our present synthesized redder colors in U-V and B-V are probably due to the absence of the PAGB and details in the evolutionary color plots are due to the first aspect. We believe that our photometric code is as good as the completeness and homogeneity restrictions allow. These aspects will be studied in future papers.

Our results confirm that models of galaxy counts for open cosmologies or for cosmologies with a non-zero cosmological constant reproduce the observed excess in the blue band counts but predict an excess in the infrared counts. The data from galaxy counts in different bands along with data from redshifts suggest strongly that we are facing an evolutionary problem. We have developed an  $\Omega_0 = 1$  model with a zero cosmological constant in which the number of galaxies we called interacting is increasing as a power law with redshift. We have found that the exponent which gives the best fit to the observations is 3.8. It implies that for each galaxy now there were 4.2 galaxies at  $z \sim 2$ , most of them interacting galaxies. Therefore, we conclude that a flat model with  $\Lambda_0 = 0$  can be a good option as long as the constant number of galaxies hypothesis is abandoned. We have used a gaussian and a Schechter representation for the luminosity function of the brighter galaxies, E/S0 and Sa-c, and a Schechter formulation for the rest of the types. It is shown that a Schechter representation works in fitting the number-redshift relation; alternatively the number of high  $z$  galaxies predicted is higher than observed when a gaussian distribution for the brighter galaxies is used.

#### ACKNOWLEDGEMENTS

We thank G. Schaller and G. Bruzual for providing us some of their models. We also thank the computing service of UNAM by allowing us to use the supercomputer CRAY YMP-4/432. We acknowledge useful conversations with Grant Mathews and Jim Truran. This work was supported in part by Universidad Nacional Autónoma de México and by the NSF, the DOE and NASA at the University of Chicago, and by the DOE and by NASA through grant 2381 at Fermilab.

#### REFERENCES

- Arimoto, N., & Yoshii, Y. 1986, A&A, 164, 260  
 Becker, S.A., & Iben, I., Jr. 1979, ApJ, 232, 831  
 Becker, S.A., & Mathews, G.J. 1983, ApJ, 270, 155  
 Bedijn, P.J. 1988, A&A, 205, 105

- Binggeli, B., Sandage, A., & Tammann, G.A. 1988, ARA&A, 26, 509 (BST)
- Broadhurst, T.J., Ellis, R.S., & Shanks, T. 1988, MNRAS, 235, 827
- Bruzual, A.G. 1983, ApJ, 273, 105
- Bruzual, A.G. 1992, private communication
- Bruzual, A.G., & Charlot, S. 1993, ApJ, 405, 538 (BCh)
- Caldwell, N., Armandroff, T.E., Seitzer, P., & Da Costa, G.S. 1992, AJ, 103, 840
- Carlberg, R.G., & Charlot, S. 1992, ApJ, 397, 5 (CCh)
- Charlot, S., & Bruzual, A.G. 1991, ApJ, 367, 126 (ChB)
- Chiosi, C. 1992, private communication
- Colin, P., & Schramm, D.N. 1993, ApJ, 407, 510
- Colles, M.M., Ellis, R.S., Taylor, K., & Hook, R.N. 1990, MNRAS, 244, 408
- Cole, S., Treyer, M.-A., & Silk, J. 1992, ApJ, 385, 9
- Coleman, G.D., Wu, C.-C., & Weedman, D.W. 1980, ApJS, 43, 393 (CWW)
- Cowie, L.L. 1993, private communication n
- Cowie, L.L., Gardner, J.P., Wainscoat, R.J., & Hodapp, K.W. 1993, remitido a ApJ
- Dyck, H.M., Zuckerman, B., Leinert, Ch., & Beckwith, S. 1974, ApJ, 189, 89
- Ferguson, H.C., & Sandage, A. 1991, AJ, 101, 765
- Flower, P.J. 1977, A&A, 54, 31
- Frogel, J.A., & Whitford, A.E. 1987, ApJ, 320, 199
- Fukugita, M., Takahara, F., Yamashita, K., & Yoshii, Y. 1990, ApJ, 361, L1
- Gilmore, G., & Wyse, R.F.G. 1991, ApJ, 367, L55
- Guiderdoni, B., & Rocca-Volmerange, B. 1987, A&A, 186, 1
- Guiderdoni, B., & Rocca-Volmerange, B. 1990, A&A, 227, 362
- Herman, J., & Habing, H.J. 1985, Phys. Rep., 124-4, 255
- Herman, J., Burger, J.H., & Phennix, W.H. 1986, A&A, 167, 247
- Johnson, H.L. 1966, ARA&A, 4, 193
- Kennicutt, R.C. 1983, ApJ, 272, 54
- Kolb, E.W., & Turner, M.S. 1990, in The Early Universe (Addison-Wesley Publishing Company).
- Koo, D.C., & Kron, R.G. 1992, ARA&A, 30, 613
- Kurucz, R.L. 1991, in Stellar Atmospheres: Beyond Classical Models, NATO ASI Series C, Vol. 341
- Lattanzio, J.C. 1986, ApJ, 311, 708
- Lee, T.A. 1970, ApJ, 162, 217
- Lilly, S.J., Cowie, L.L., & Gardner, J.P., 1991, ApJ, 369, 79
- Maddox, S.J., Sutherland, W.J., Efsthathiou, G., Loveday, J., & Peterson, B.A. 1990, MNRAS, 247, 1P
- Maeder, A. 1992, private communication

- Maeder A., & Meynet, G. 1989, A&A, 210, 155 (MM)
- Mathews, G.J., & Schramm, D.N. 1993, ApJ, 404, 468
- Metcalf, N., Shanks, T., Fong, R., & Jones, L.R. 1990, MNRAS, 249, 498
- Pence, W. 1976, ApJ, 203, 39
- Renzini, A. 1993, preprint
- Reid, N., Tinney, C., & Mould, J. 1990, ApJ, 348, 98
- Rogers, F.J., & Iglesias, C.A. 1992, ApJS, 79, 507
- Sandage, A., Bingelli, B., & Tammann, G.A. 1985, AJ, 90, 1759 (SBT)
- Seidel, E., Demarque, P., & Weinberg, D. 1987, ApJS, 63, 917
- Schaller, G., Schaerer, D., Meynet, G., & Maeder, A. 1992, A&AS, 96, 269 (SSMM)
- Schechter, P. 1976, ApJ, 203, 29
- Tinsley, B.M. 1972, A&A, 20, 383
- Tinsley, B.M. 1976, ApJ, 208, 797
- Tinsley, B.M. 1980, FunCosP, 5, 287
- Tinsley, B.M., & Gunn, J.E. 1976, ApJ, 203, 52
- Toomre, A. 1977, in Evolution of Galaxies and Stellar Populations, ed. B.M. Tinsley, & R.B. Larson (New Haven: Yale Observatory), 401
- Turnshek, et al. 1989, ApJ, 344, 567
- Tyson, J.A. 1988, AJ, 96, 1
- VandenBerg, D.A., Hartwick, F.D.A., Dawson, P., & Alexander, D.R. 1983, ApJ, 266, 747
- Wang, B. 1991, ApJ, 383, L37
- Wheeler, J.C., Sneden, C., & Truran, J.W. 1989, ARA&A, 27, 279
- Yoshii, Y. 1993, ApJ, 403, 552
- Yoshii, Y., & Takahara, F. 1988, ApJ, 326, 1 (YT)

## FIGURE CAPTIONS

- Fig. 1.—(a-b) Evolution of the color indexes B-V and V-K for a burst, constant, and exponentially decreasing ( $\tau = 0.5$  Gyr) star formation rate (SFR). With  $O_J$  we have denoted our model with the Johnson (1966) calibration whereas 1 Gyr, cons., or exp. means 1 Gyr burst, constant, or exponentially decreasing SFR. Denoted by B are the corresponding models of Bruzual & Charlot (1993).
- Fig. 2.—(a-b) As in the former figure, here we have plotted the B-V and V-K evolution for different SFRs. In this case, we have added two more curves (for each figure), the 1 Gyr and constant  $O_B$  models. We have not plotted the exponentially decreasing model. With  $O_B$  we have denoted our models with the Bruzual low-temperature photometric calibration (Bruzual 1992).
- Fig. 3.—(a-b) Evolution of the color indexes B-V and V-K for two SFRs: the 1 and 0.1 Gyr burst SFR.
- Fig. 4.—(a-b) Evolution of the color indexes B-V and V-K for three different SFRs: the NMS, the OMS, and a constant SFR.
- Fig. 5.—(a-b) Two V-K vs. B-V color-color diagrams with different SFRs. In Fig. 5a we have plotted the 1 Gyr burst SFR models. As before, with  $O_{J(B)}$  we have denoted our model with Johnson (Bruzual) calibration. The data are from Yoshii & Takahara (1988) with estimated uncertainties. The triangles, squares, and ten-pointed stars lying on the curves are the models at the age indicated by the numbers in Gyr. The four-pointed star is a model, at the age of 15 Gyr, using the low-mass tracks of Chiosi (1992). In Fig. 5b the time development of the models with the NMS, OMS, cons., and exp. SFRs in the B-V versus V-K diagram is plotted.
- Fig. 6.— Spectral energy distributions for the different types of galaxies considered here from Coleman, Wu, & Weedman (1980) and Pence (1976). They are supplemented by our photometric evolution of galaxies model.
- Fig. 7.—(a-f) The k and e corrections and the sum of both in the B and K color band are plotted here. We have used an exponentially decreasing SFR with five time-scales to represent the five different classes of galaxies: Sdm ( $\tau = \infty$  Gyr), Scd ( $\tau = 9.0$  Gyr), Sbc ( $\tau = 5.0$  Gyr), Sab ( $\tau = 3.0$  Gyr), and E/SO ( $\tau = 0.5$  Gyr). The cosmology assumed is that with  $(\Omega_m, \Omega_v) = (1, 0)$  and  $z_F = 3.0$ .
- Fig. 8.— “Passive” evolution of the luminosity function of galaxies (LFG) for a flat universe and zero cosmological constant. The hypothesis of universality has been assumed. Here we have assumed a conservation in the number of galaxies, per comoving volume.
- Fig. 9.— Number of galaxies versus apparent blue magnitude assuming universality for the LFG. The observations are from Maddox et al. (1990), Metcalfe et al. (1991), and Lilly et al. (1991). The different lines cover evolving (E) and nonevolving (NE) models for three different cosmologies.
- Fig. 10.— Number of galaxies versus apparent blue magnitude for the evolving  $(\Omega_m, \Omega_v) = (1, 0)$  model of the last figure. Explicitly plotted are the contributions to the number for different types of galaxies.
- Fig. 11.— As in Fig. 10, here we have also plotted an evolving  $(\Omega_m, \Omega_v) = (1, 0)$  model with the contributions of the different type of galaxies. However, unlike the model of Fig. 10, the universality hypothesis has been abandoned and now the Schechter parameters  $\alpha$  and  $M_B^*$  are vectors (Carlberg & Charlot 1992).
- Fig. 12.— Number-apparent magnitude relation in the infrared K band for the same models of Fig. 3.4. Data are from a compilation of Cowie (1993).

- Fig. 13.— Redshift distribution of galaxies in a fixed interval of apparent blue magnitude. The models are again the same as those of Figs. 9 and 12 except for what we called Schechter model (see also Fig. 11). Data are from Broadhurst, Ellis, & Shanks (1988).
- Fig. 14.—(a–b) Number versus apparent blue magnitude for our merger model with two representations of the luminosity function of the brighter galaxies (Sa-c and E/SO): (a) the gaussian formulation, and (b) the Schechter representation. Aside from this and the value of the normalization parameter, both models have the same values of the parameters.
- Fig. 15.—(a–b) Number versus apparent K magnitude for the same merger model.
- Fig. 16.—(a–b) Redshift distribution for our model with the two luminosity function representations in two apparent blue magnitude intervals. Data are again from Broadhurst, Ellis, & Shanks (1988).

TABLE 1

## OBSERVED (O) AND SYNTHESIZED COLORS OF E/SO GALAXIES

| SFR <sup>a</sup> | M/Ch <sup>b</sup> | U-V  | B-V  | V-R  | V-I  | V-J  | V-K  | V-L  |
|------------------|-------------------|------|------|------|------|------|------|------|
| O                |                   | 1.40 | ...  | ...  | ...  | ...  | 3.22 | ...  |
| O                |                   | 1.50 | 0.96 | 0.84 | 1.59 | 2.37 | 3.31 | ...  |
| O                |                   | ...  | 0.97 | 0.86 | 1.61 | 2.20 | 3.20 | ...  |
| O                |                   | ...  | 0.97 | 0.89 | 1.70 | 2.47 | 3.39 | 3.56 |
| O                |                   | 1.33 | ...  | ...  | ...  | 2.36 | 3.26 | ...  |
| B= 1 Gyr         | M                 | 1.88 | 1.08 | 0.90 | 1.63 | 2.42 | 3.26 | 3.48 |
| B= 1 Gyr         | Ch                | 1.76 | 1.04 | 0.87 | 1.57 | 2.32 | 3.23 | 3.46 |

<sup>a</sup>The SFR we took to simulate an elliptical galaxy has a 1 Gyr burst; i.e, a SFR which is constant during the first gigayear and zero henceforth.

<sup>b</sup>In addition to the tracks by Maeder (M) (Schaller et al. 1993) we have also used low-mass tracks, provided kindly by Dr. Chiosi, to compute colors at the age of the Galaxy (Ch).

TABLE 2

## OBSERVED (O) AND SYNTHESIZED (S) COLORS OF PRESENT GALAXIES

| Type | O/S | U-V  | B-V  | V-R  | V-I  | V-J  | V-K  | V-L  |
|------|-----|------|------|------|------|------|------|------|
| E/SO | O   | 1.40 | ...  | ...  | ...  | ...  | 3.22 | ...  |
|      | O   | 1.50 | 0.96 | 0.84 | 1.59 | 2.37 | 3.31 | ...  |
|      | O   | ...  | 0.97 | 0.86 | 1.61 | 2.20 | 3.20 | ...  |
|      | O   | ...  | 0.97 | 0.89 | 1.70 | 2.47 | 3.39 | 3.56 |
|      | O   | 1.33 | ...  | ...  | ...  | 2.36 | 3.26 | ...  |
|      | S   | 1.76 | 1.03 | 0.87 | 1.58 | 2.34 | 3.14 | 3.37 |
| Sab  | O   | 1.07 | ...  | ...  | ...  | ...  | 3.18 | ...  |
|      | O   | 0.89 | 0.79 | 0.86 | ...  | ...  | ...  | ...  |
|      | S   | 1.27 | 0.86 | 0.80 | 1.51 | 2.23 | 2.99 | 3.27 |
| Sbc  | O   | 0.71 | ...  | ...  | ...  | ...  | 3.06 | ...  |
|      | O   | 0.55 | 0.64 | 0.66 | ...  | ...  | ...  | ...  |
|      | S   | 0.92 | 0.72 | 0.73 | 1.44 | 2.12 | 2.82 | 3.15 |
| Scd  | O   | 0.45 | ...  | ...  | ...  | ...  | 2.74 | ...  |
|      | O   | 0.37 | 0.54 | 0.62 | ...  | ...  | ...  | ...  |
|      | S   | 0.69 | 0.62 | 0.67 | 1.37 | 2.02 | 2.67 | 3.04 |
| Sdm  | O   | 0.23 | ...  | ...  | ...  | ...  | 2.32 | ...  |
|      | O   | 0.37 | 0.52 | 0.53 | ...  | ...  | ...  | ...  |
|      | S   | 0.47 | 0.50 | 0.60 | 1.29 | 1.89 | 2.47 | 2.82 |

TABLE 3

PARAMETERS OF THE NUMBER-MAGNITUDE RELATION

| $\Omega_m$ | $\Omega_v$ | h   | $z_F$ | TFE <sup>a</sup> IMF <sup>b</sup> | $n_{lg}$ <sup>c</sup> | $\phi^*(1 \times 10^{-3})$ | $\alpha$            | $M_\lambda^*$       | Mix <sup>d</sup> | Universal <sup>e</sup> |
|------------|------------|-----|-------|-----------------------------------|-----------------------|----------------------------|---------------------|---------------------|------------------|------------------------|
| 1.0        | 0.0        | 0.5 | 3.    | exp 1.35                          | 5                     | 1.95                       | -1.11               | $B_J = -21.1$       | Tinsley          | Yes                    |
| 0.1        | 0.0        | 0.5 | 3.    | exp 1.35                          | 5                     | 1.95                       | -1.11               | $B_J = -21.1$       | Tinsley          | Yes                    |
| 0.38       | 0.62       | 0.5 | 3.    | exp 1.35                          | 5                     | 1.95                       | -1.11               | $B_J = -21.1$       | Tinsley          | Yes                    |
| 1.0        | 0.0        | 0.5 | 3.    | exp 1.35                          | 5                     | 6.48                       | vector <sup>1</sup> | vector <sup>2</sup> | CCh              | No                     |

<sup>a</sup>The star formation rate considered here is exponentially decreasing:  $\psi \propto e^{-t/\tau}$ .

<sup>b</sup>We have assumed as initial mass function a power law:  $\phi \propto m^{-(1+z)}$ .

<sup>c</sup>We have classified galaxies in five different categories (Pence 1976, Tinsley 1980).

<sup>d</sup>It has been used the relative contributions from Tinsley (1980) and Carlberg & Charlot (1992): (E/SO, Sab, Sbc, Scd, Sdm) = (0.321, 0.281, 0.291, 0.045, 0.061) and (0.185, 0.065, 0.167, 0.157, 0.426), respectively.

<sup>e</sup>Universal means that the shape of the luminosity function (LF) for each group of galaxies does not change with type; in particular, in the Schechter (1976) formulation for the LF it means that the values of the parameters  $\alpha$  y  $M^*$  do not vary.

<sup>1</sup> $\vec{\alpha} = (-0.5, -1.0, -1.25, -1.5, -1.5)$ .

<sup>2</sup> $\vec{M}_B^* = (-21.1, -20.0, -19.0, -18.0, -16.0)$ .

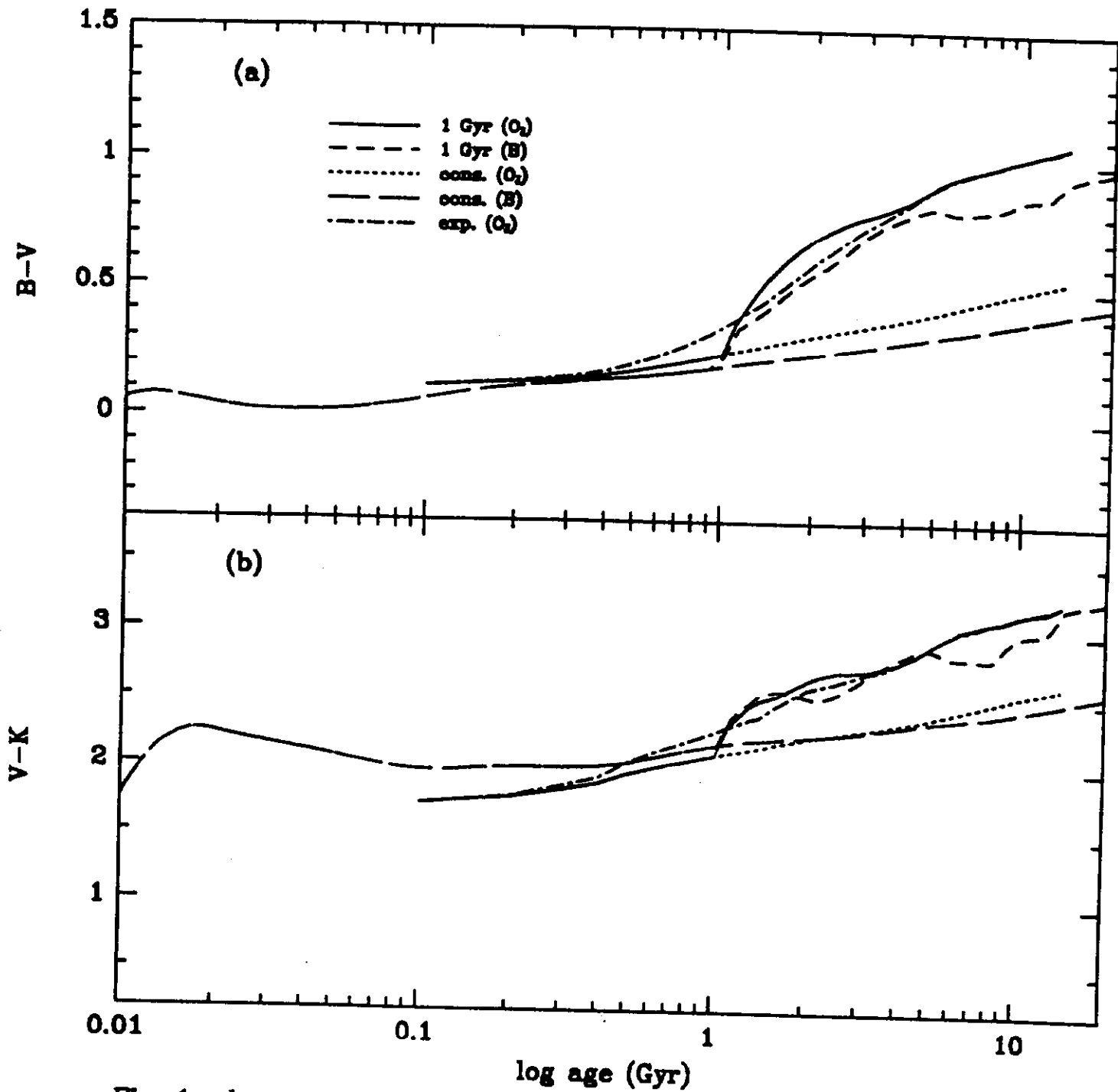


Fig. 1a-b

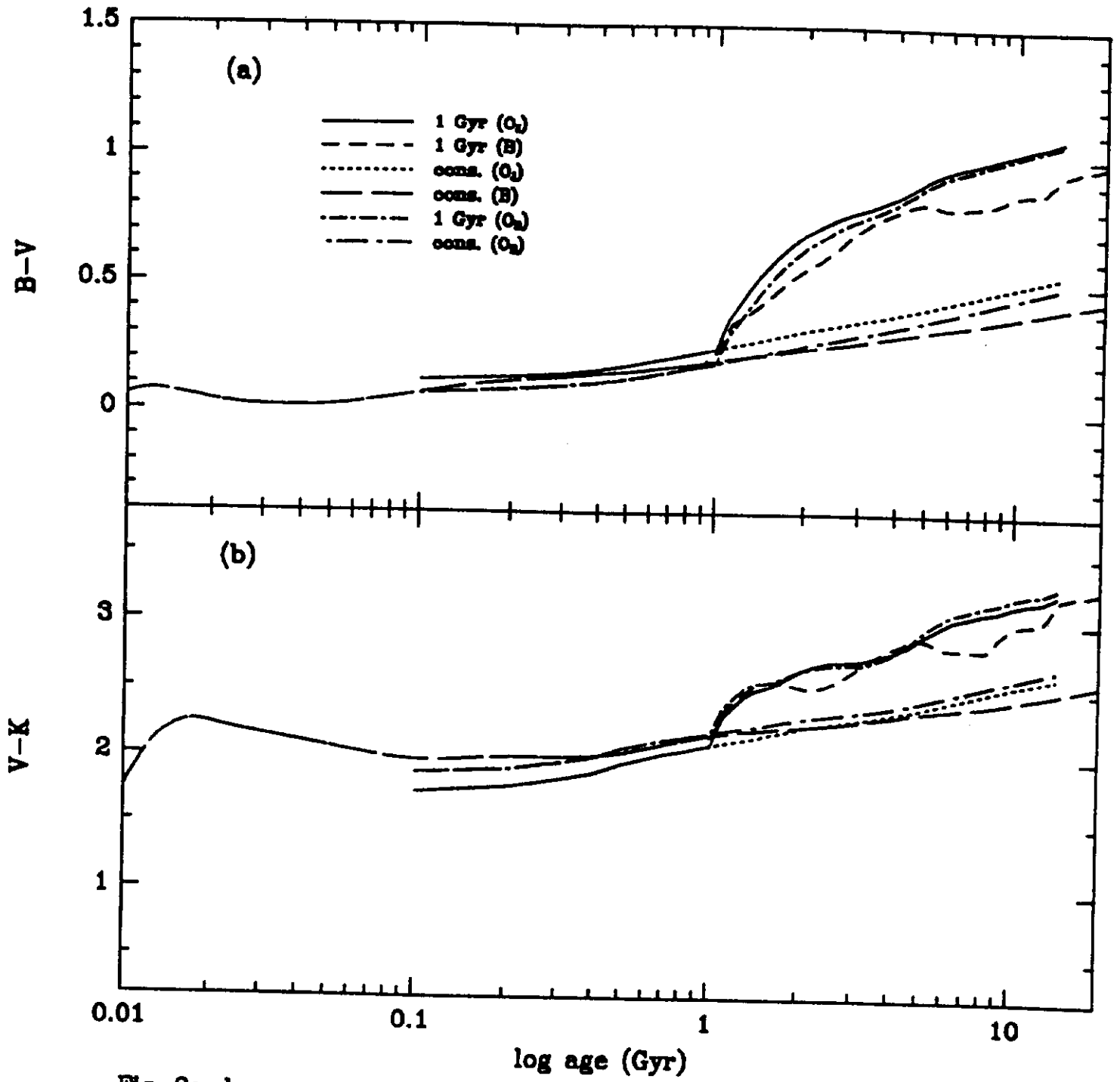


Fig. 2a-b

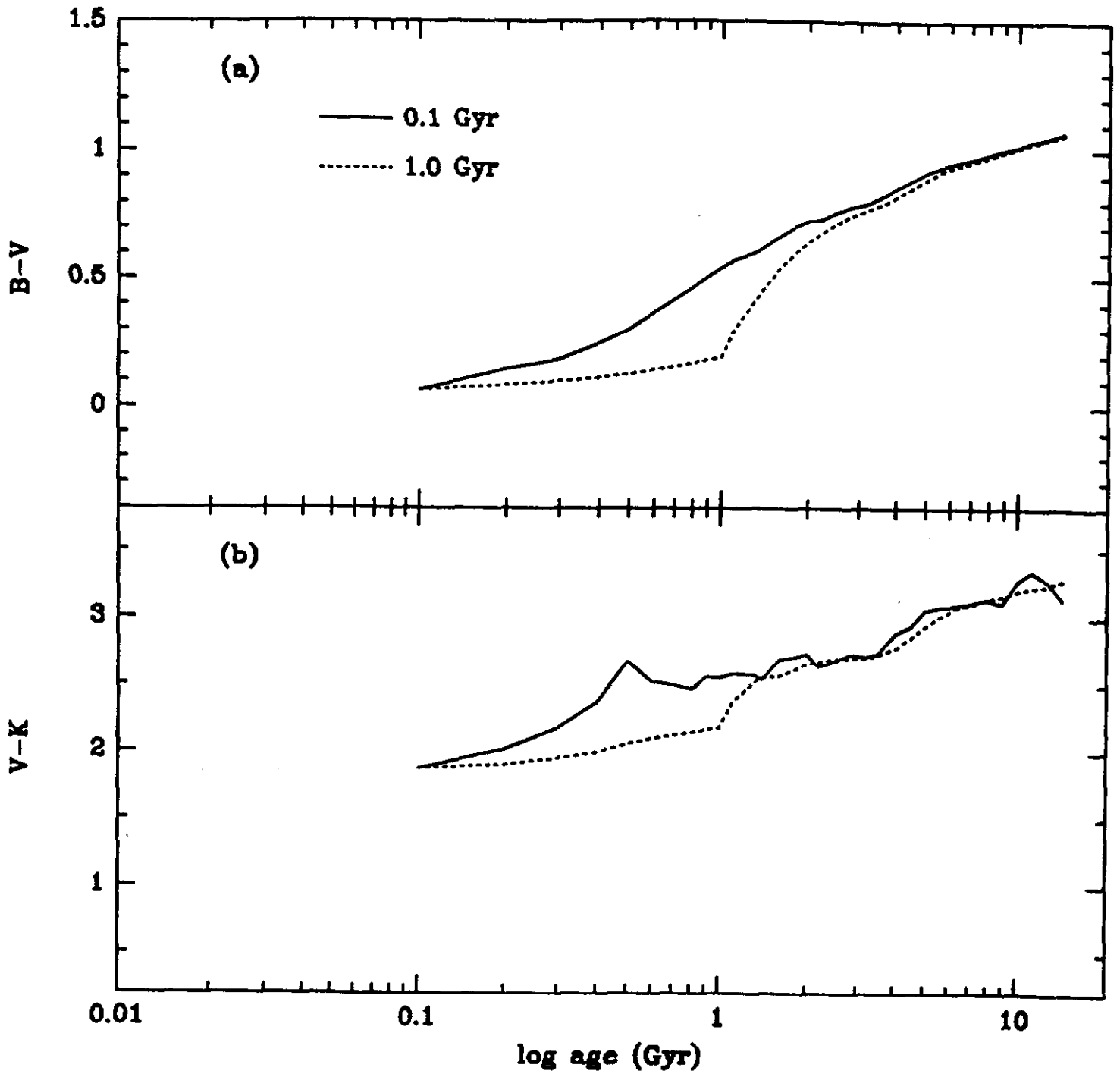


Fig. 3a-b

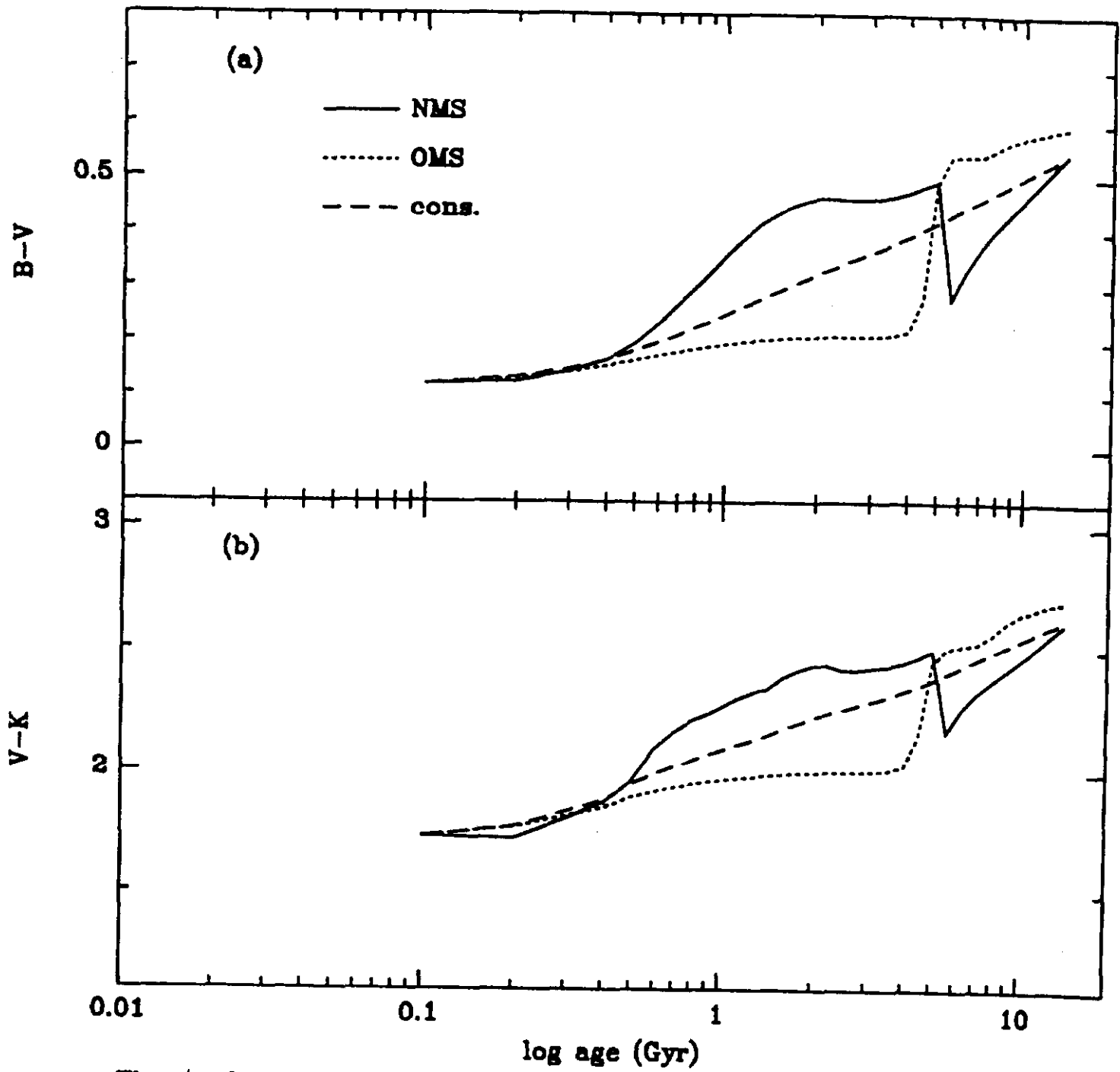


Fig. 1/a-b

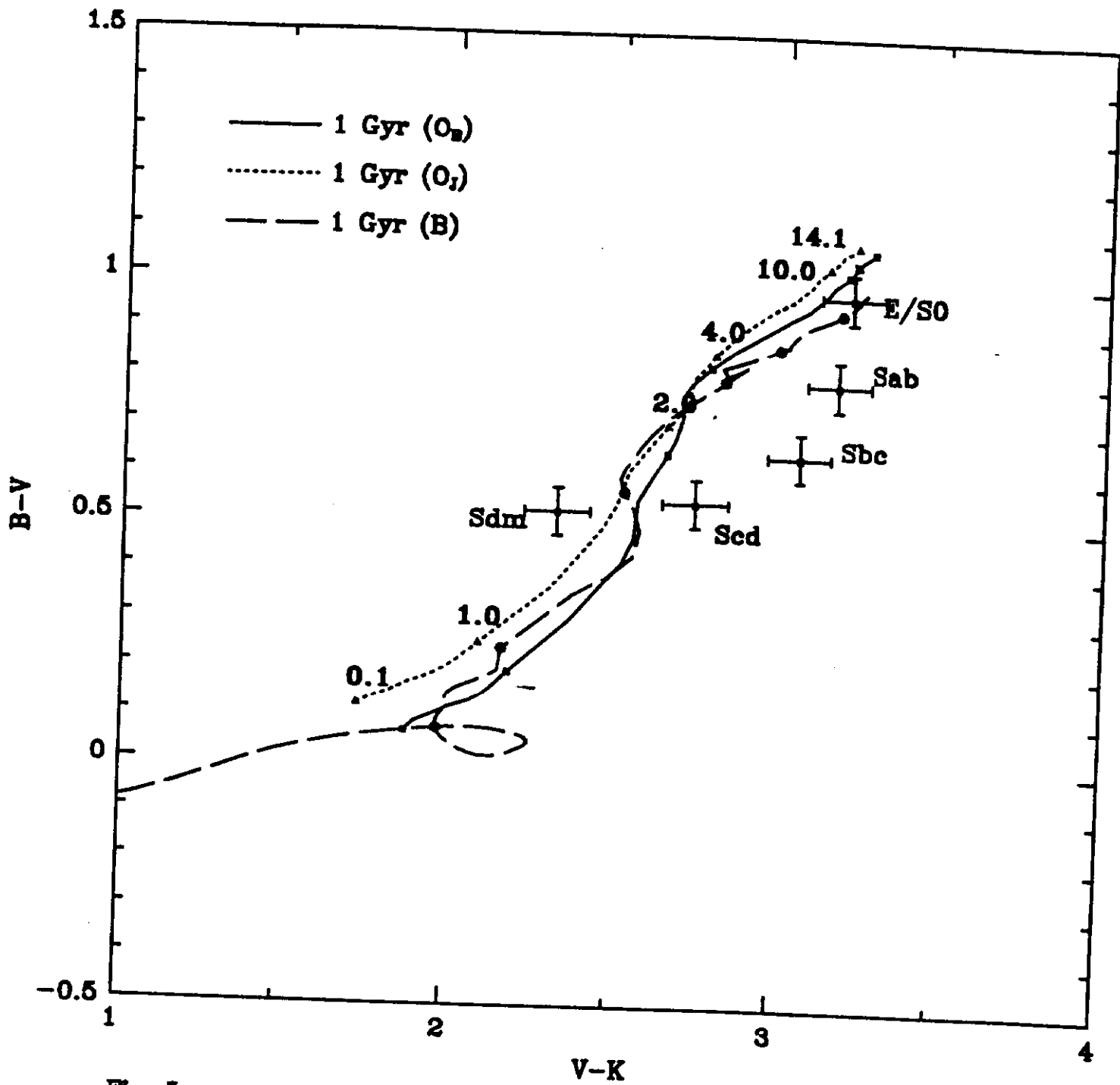


Fig. 5a

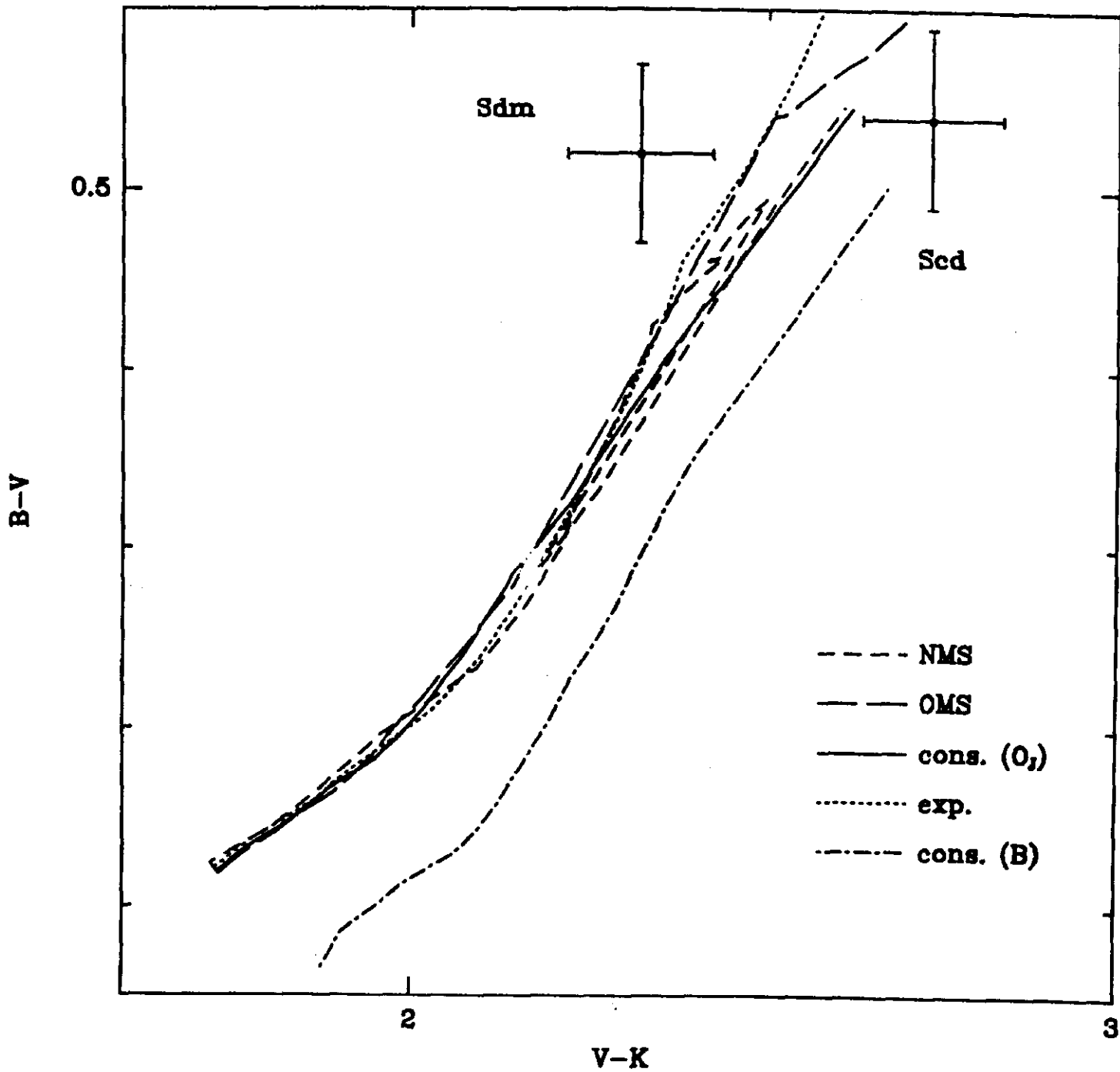


Fig. 5b

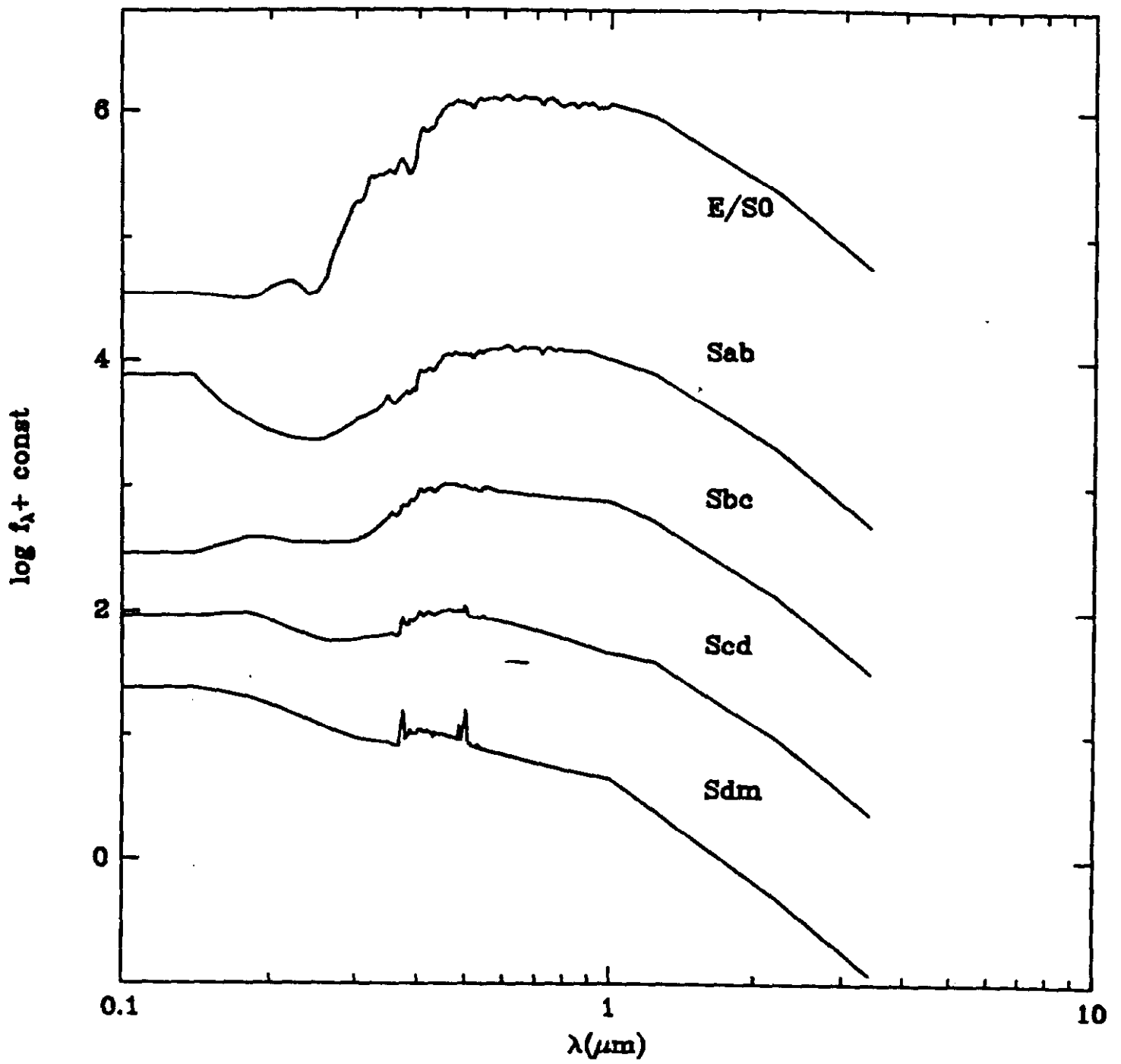


Fig. 6

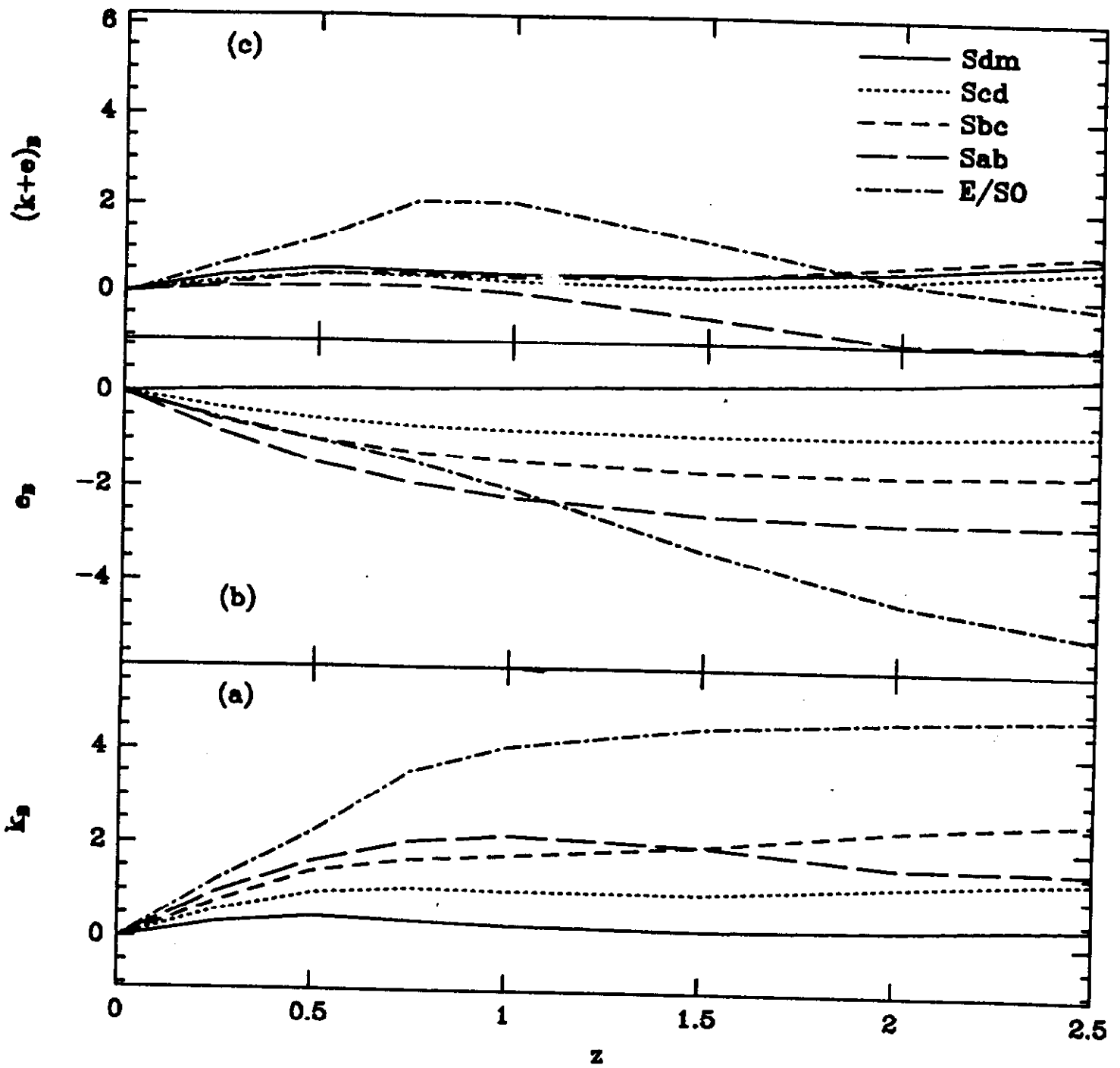


Fig. 7a-c

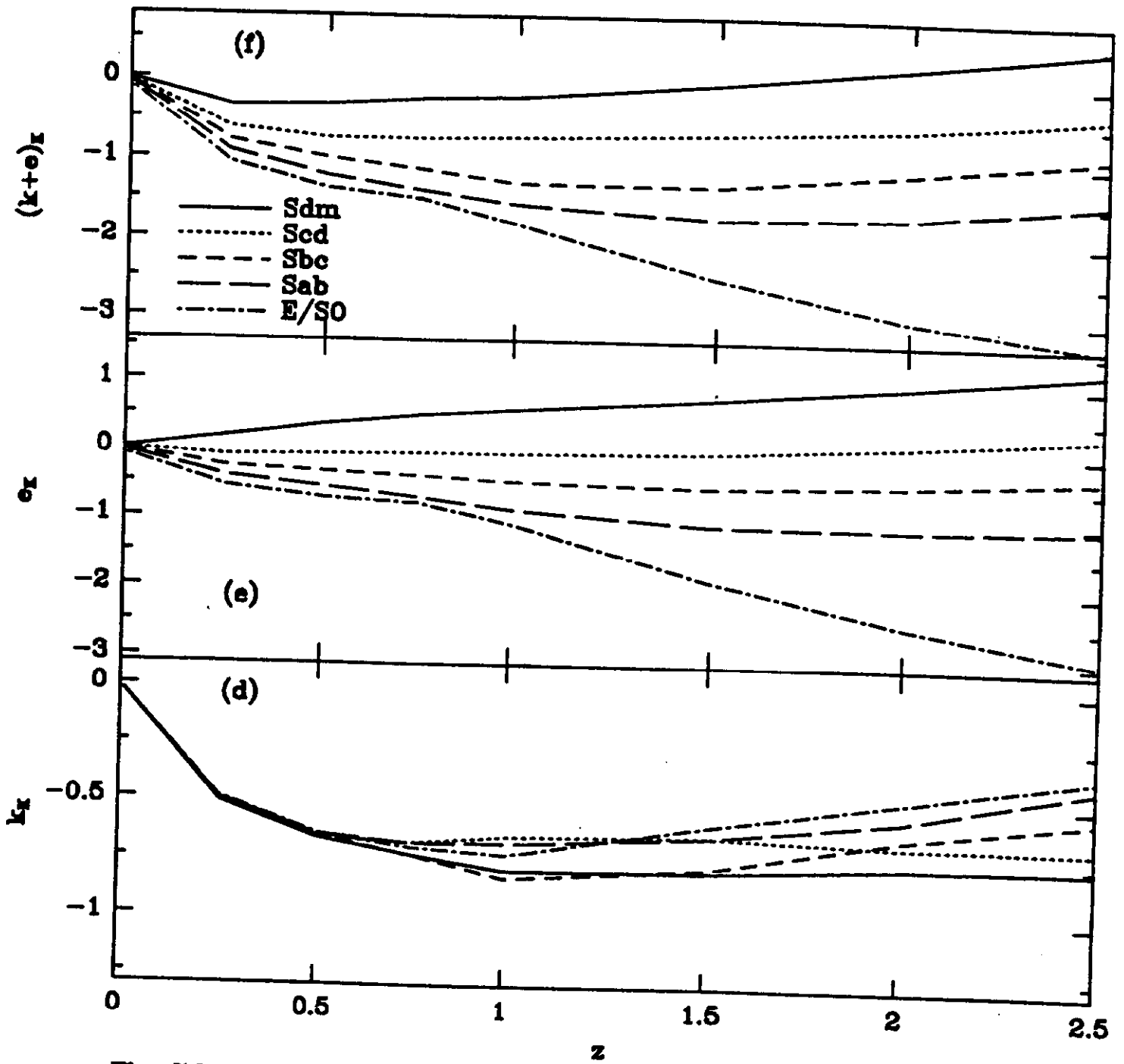


Fig. 7d-f

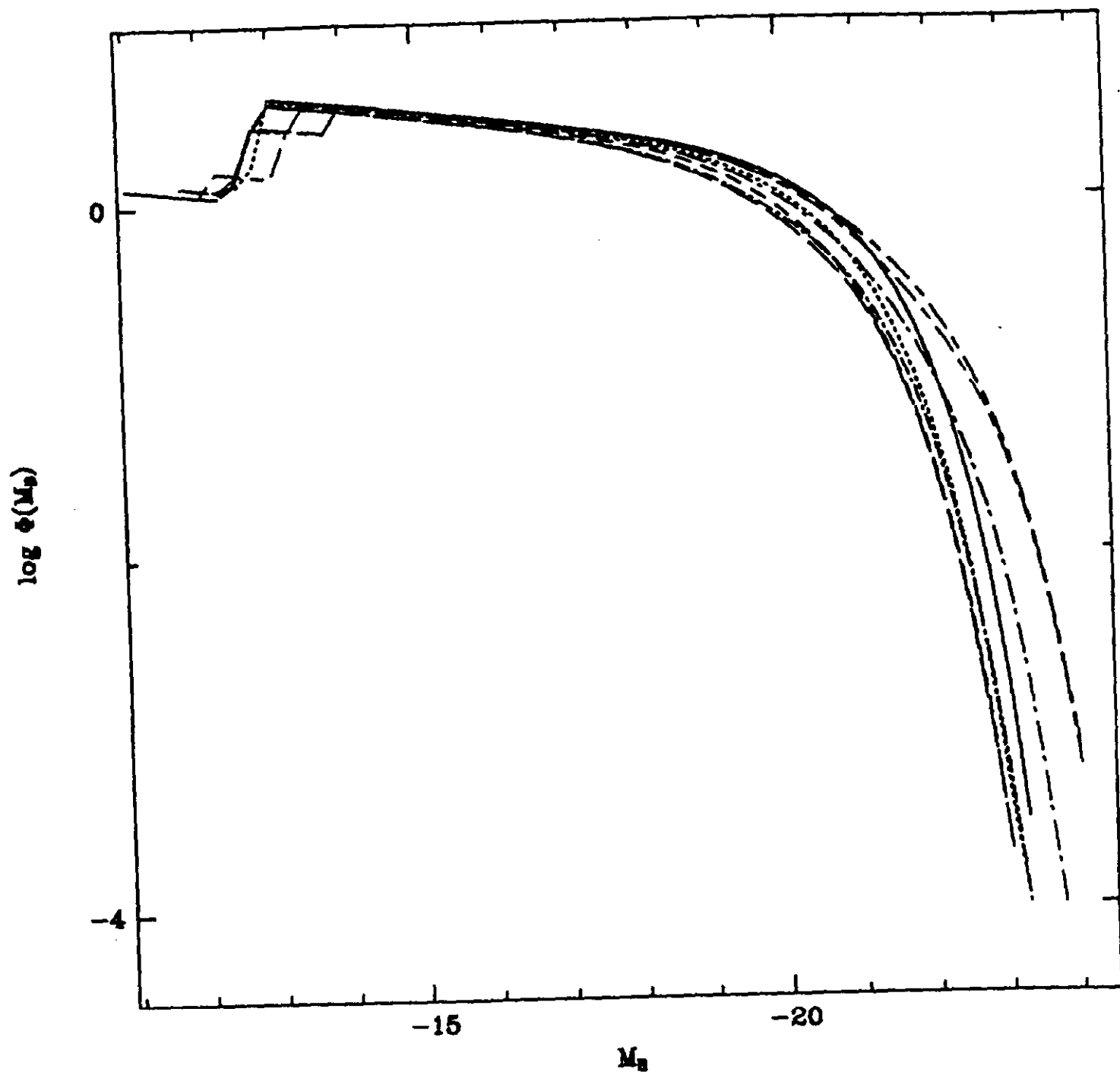


Fig. 8

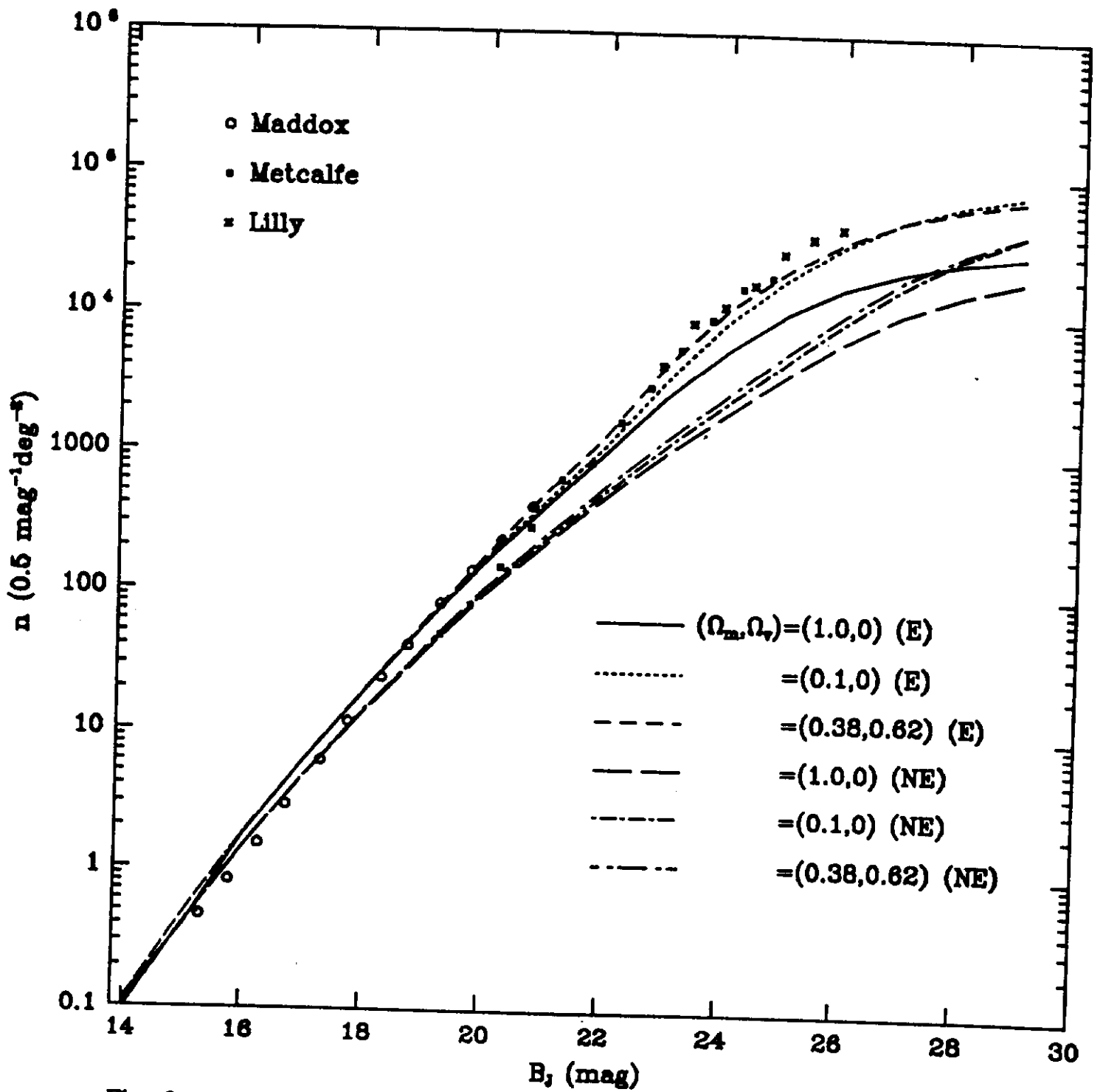


Fig. 9

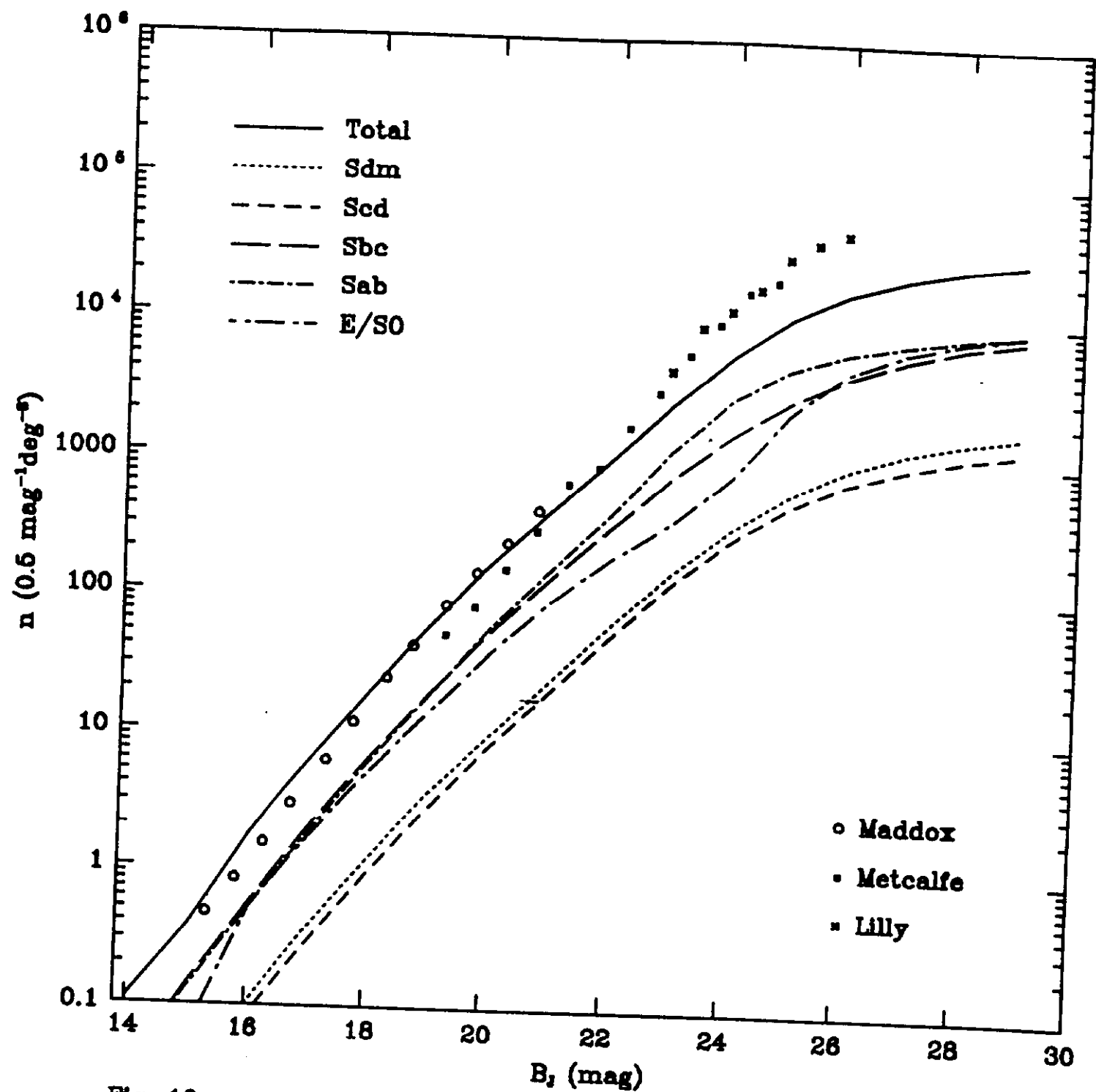


Fig. 10

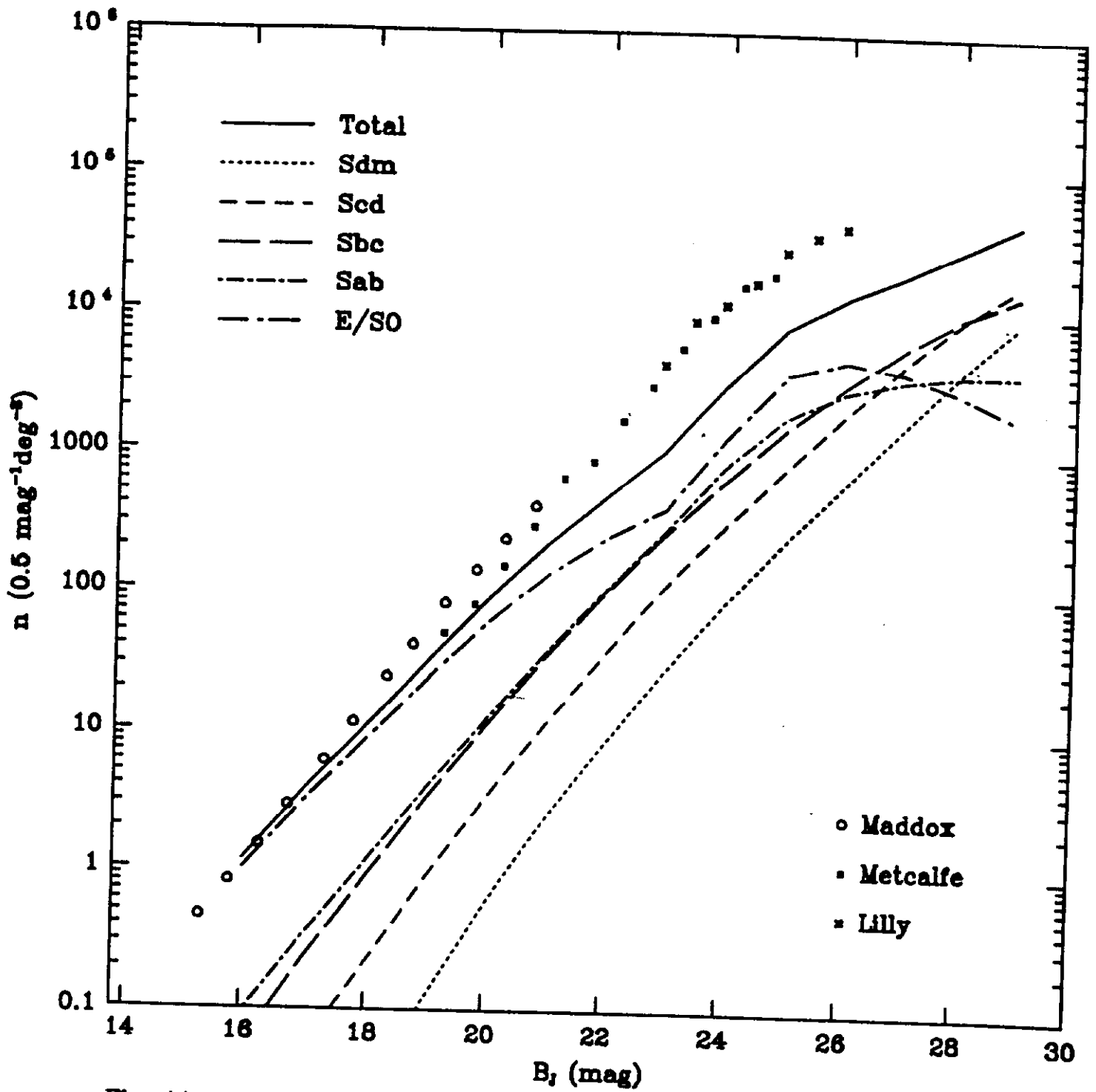


Fig. 11

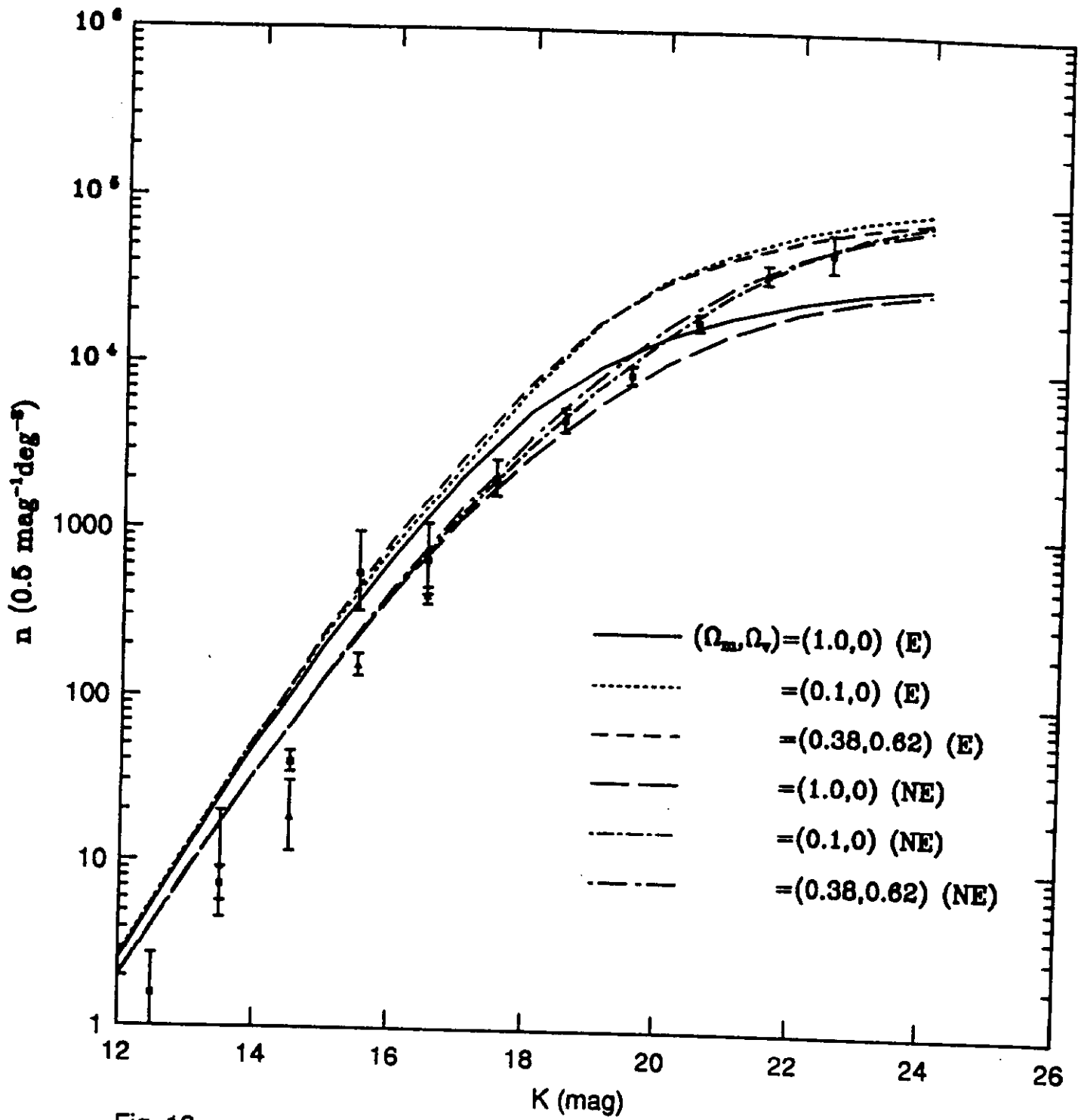


Fig. 12

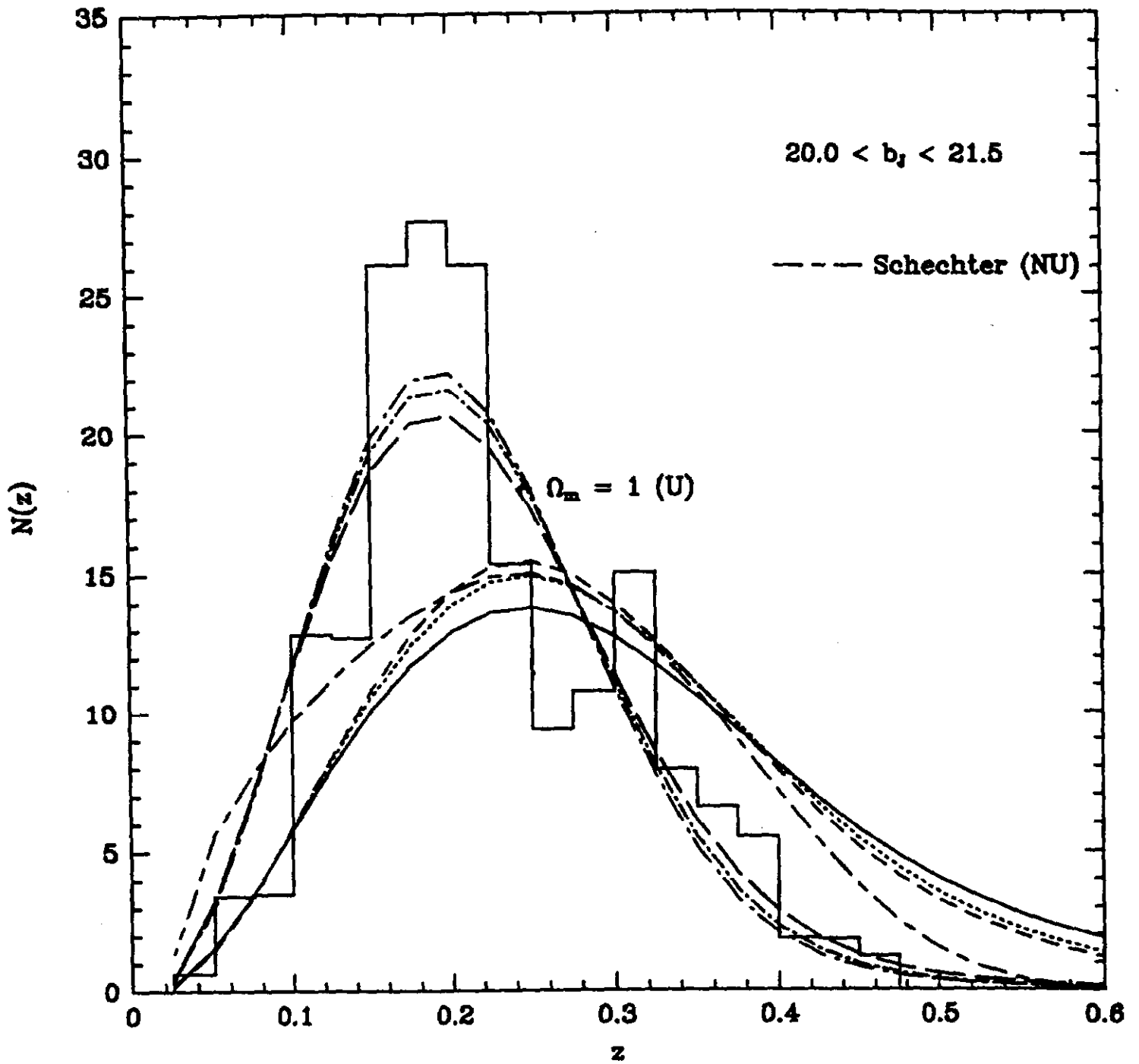


Fig. 13

$n$  ( $0.5 \text{ mag}^{-1} \text{deg}^{-2}$ )

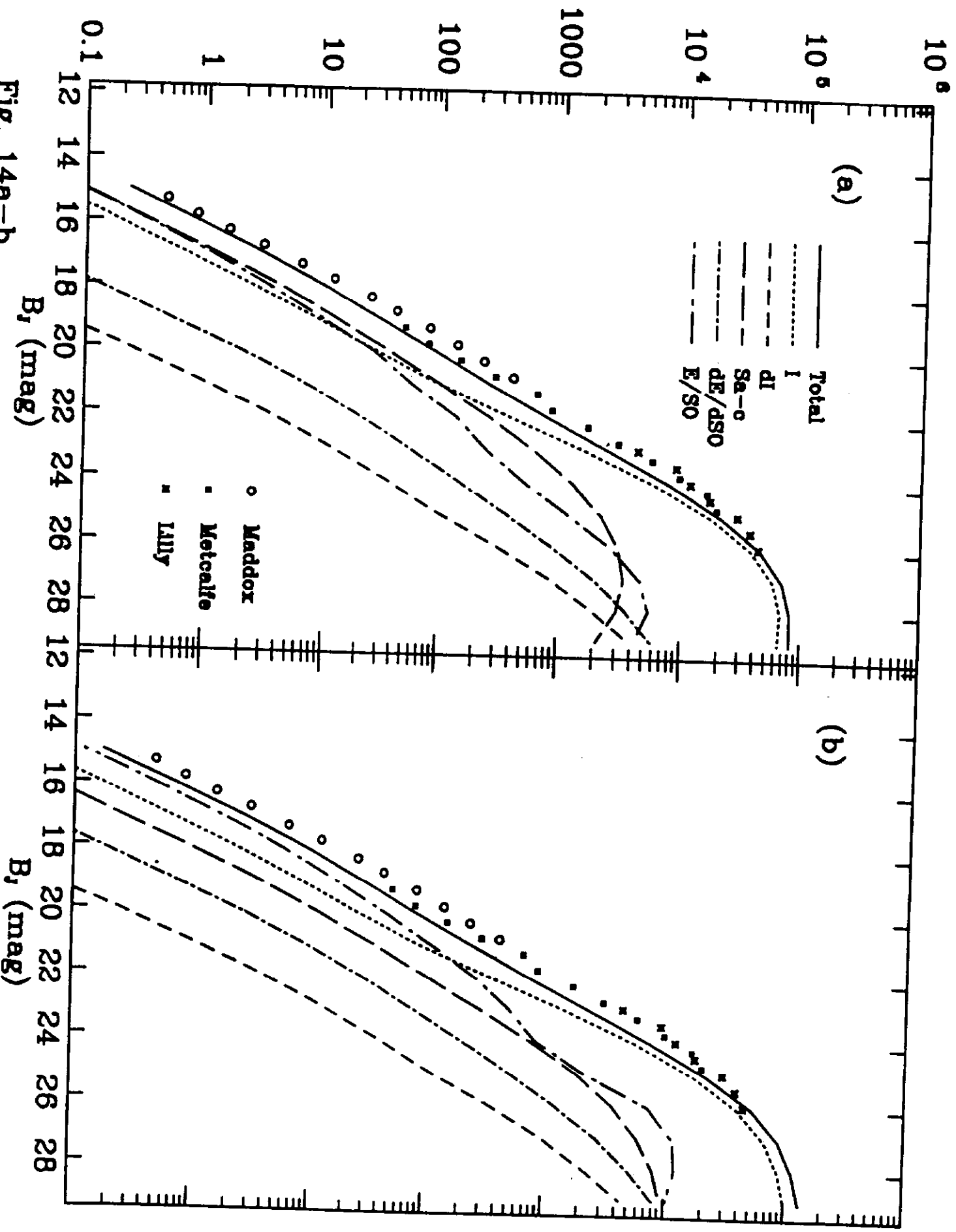


Fig. 14a-b

$n$  ( $0.5 \text{ mag}^{-1} \text{deg}^{-2}$ )

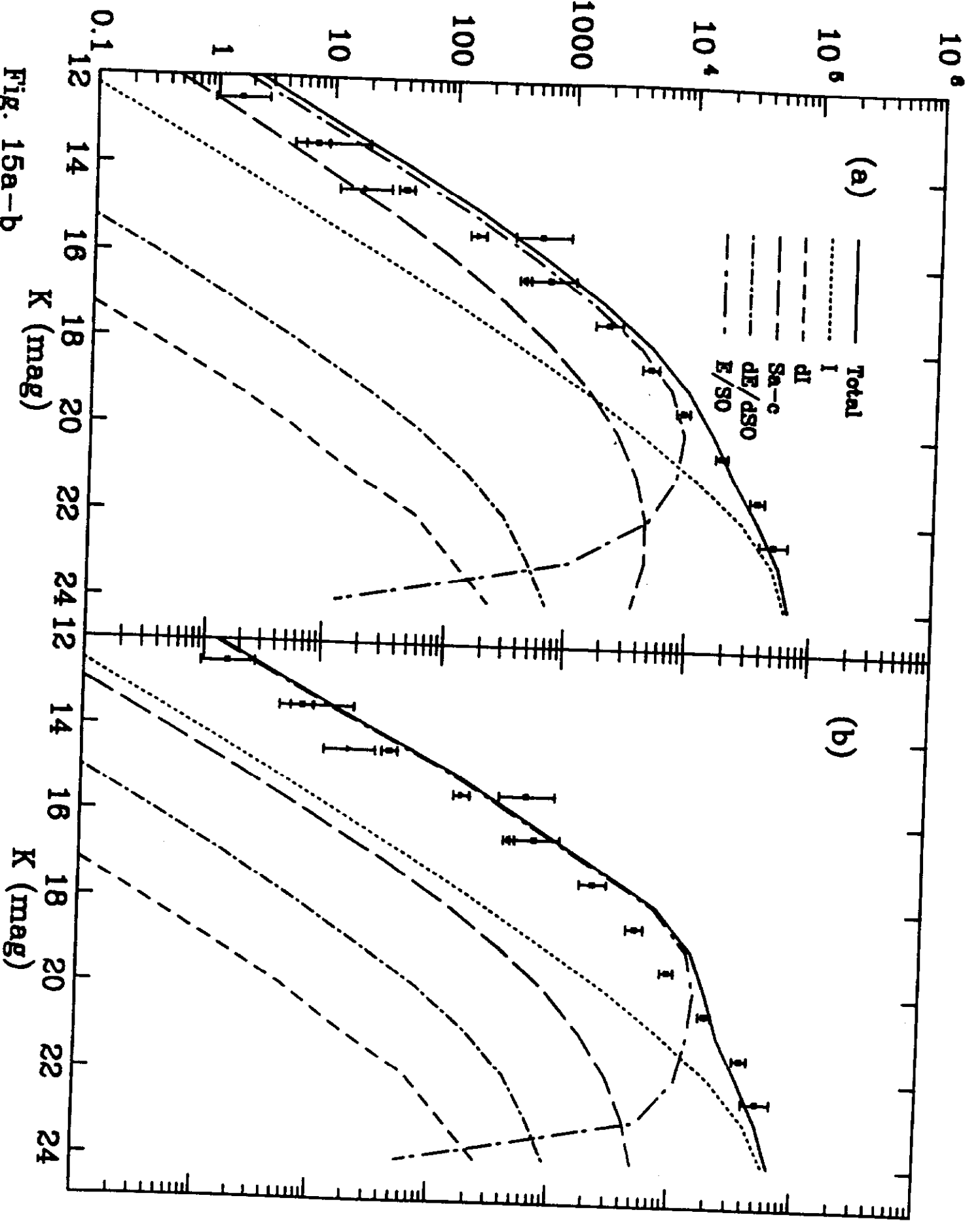


Fig. 15a-b

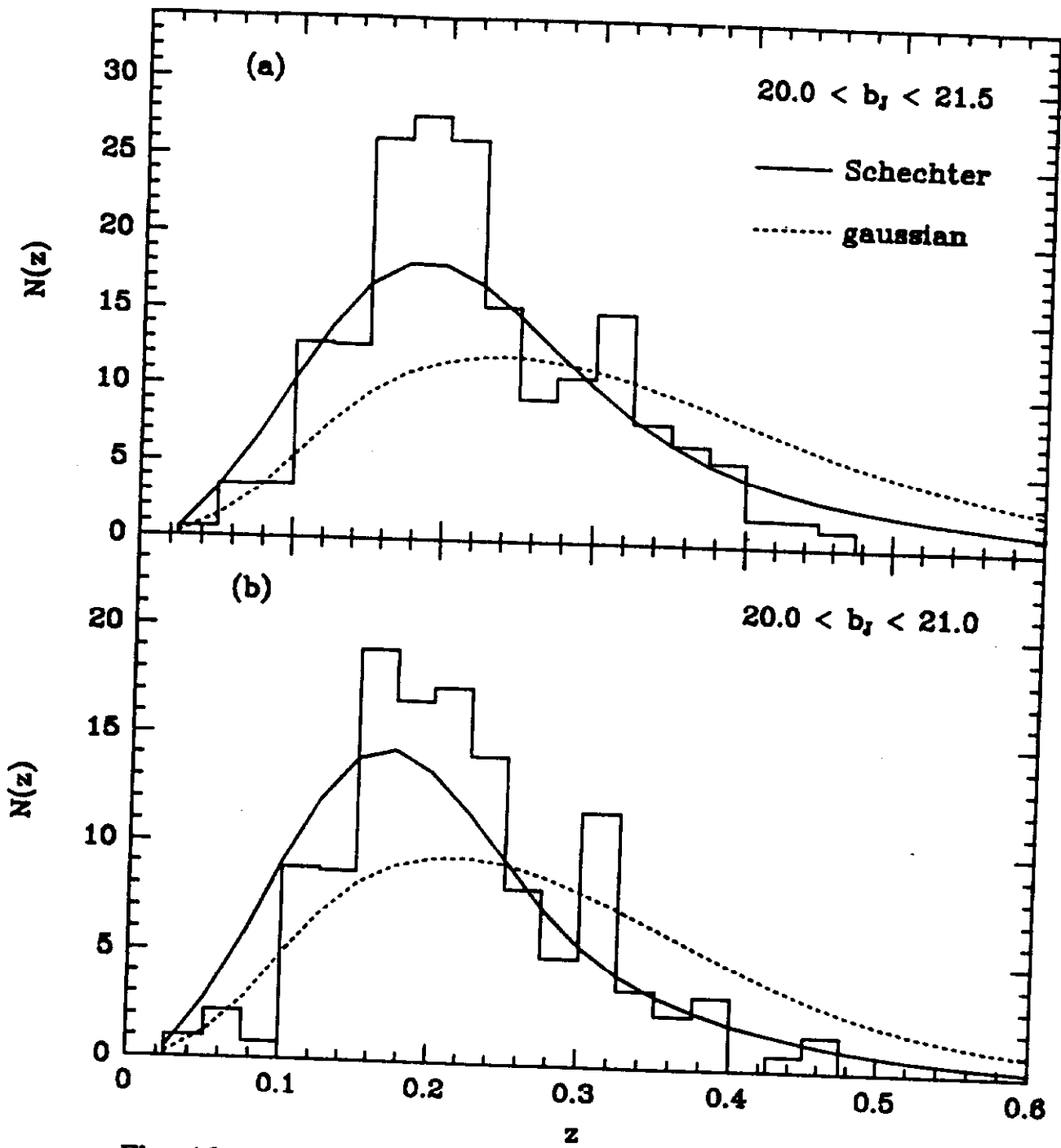


Fig. 18a-b